# Journal Pre-proof


Single cell transcriptomics of human weight loss links adipocyte NPY1R to control of lipolysis

Julius E.R. Grothen, Jaime M. Martinez, Nikos Sidiropoulos, Lucas Massier, Danae Zareifi, Jiawei Zhong, Ida Davidsen, Jette W. Platou, Jette Mandelbaum, Pia Rothe, Henning Hvid, Mads Grønborg, Christian Toft Madsen, Jens M. Bruun, Mikael Rydén, Niklas Mejhert, Jørn W. Helge, Zachary Gerhart-Hines, Thomas Å. Pedersen

PII: S2212-8778(25)00212-1

DOI: https://doi.org/10.1016/j.molmet.2025.102305

Reference: MOLMET 102305

To appear in: *Molecular Metabolism*

Received Date: 15 October 2025

Revised Date: 2 December 2025

Accepted Date: 10 December 2025

Please cite this article as: Grothen JER, Martinez JM, Sidiropoulos N, Massier L, Zareifi D, Zhong J, Davidsen I, Platou JW, Mandelbaum J, Rothe P, Hvid H, Grønborg M, Madsen CT, Bruun JM, Rydén M, Mejhert N, Helge JW, Gerhart-Hines Z, Pedersen TÅ, Single cell transcriptomics of human weight loss links adipocyte NPY1R to control of lipolysis, *Molecular Metabolism*, https://doi.org/10.1016/j.molmet.2025.102305.

# Single cell transcriptomics of human weight loss links adipocyte NPY1R to control of lipolysis

Julius E. R. Grothen[1, 2], Jaime M. Martinez[1], Nikos Sidiropoulos[1], Lucas Massier[3,4], Danae Zareifi[3], Jiawei Zhong[3], Ida Davidsen[1], Jette W. Platou[1], Jette Mandelbaum[1], Pia Rothe[1], Henning Hvid[1], Mads Grønborg[1], Christian Toft Madsen[1], Jens M. Bruun[5, 6, 7], Mikael Rydén[5, 8], Niklas Mejhert[5, 8], Jørn W. Helge[9], Zachary Gerhart-Hines[2,10], and Thomas Å. Pedersen[1,10].

[1] Novo Nordisk A/S, Research & Development, Måløv, Denmark

[2] Novo Nordisk Foundation Center for Basic Metabolic Research, University of Copenhagen, Copenhagen, Denmark

[3] Department of Medicine (H7), Karolinska Institutet, C2-94, Karolinska University Hospital, Huddinge

[4] Helmholtz Institute for Metabolic, Obesity and Vascular Research (HI-MAG) of the Helmholtz Zentrum München at the University of Leipzig and University Hospital Leipzig, Leipzig, Germany

[5] Steno Diabetes Center Aarhus, Aarhus University Hospital, Aarhus, Denmark

[6] Danish National Center for Obesity, Aarhus, Denmark

[7] Department of Clinical Medicine, Aarhus University, Aarhus, Denmark

[8] Steno Diabetes Center, Copenhagen, Denmark

[9] Department of Biomedical Sciences, University of Copenhagen, Copenhagen, Denmark

[10] Corresponding authors

Correspondence should be addressed to Zachary Gerhart-Hines, Blegdamsvej 3B, 7.6.56, 2200 Copenhagen, Denmark, email: zpg@sund.ku.dk and Thomas Åskov Pedersen, Novo Nordisk Park 1, 2760 Måløv, Denmark, email: tqpe@novonordisk.com

# Abstract

**Background:**

Combination of increased physical exercise and hypocaloric diet has long been recognized to improve cardiometabolic health and adipose tissue function, including lipid turnover. How such lifestyle interventions mediate benefits at the cellular level remains unknown. Given the critical role of subcutaneous white adipose tissue (scWAT) to systemic metabolic homeostasis, we set out to interrogate how exercise and diet lifestyle intervention impacted scWAT in individuals living with obesity, with a particular focus on lipolytic capacity and cell-specific gene profiling.

**Methods:**

Single nuclei RNA sequencing (snRNAseq) was performed on cryopreserved scWAT biopsies originally collected before and after lifestyle intervention, involving regular exercise and hypocaloric diet in obese individuals. Findings on regulation of lipolysis in adipocytes were followed up with meta-analysis of clinical studies and pharmacological experiments in mature human adipocytes.

**Results:**

snRNAseq analysis revealed intervention-induced changes in all scWAT cell-types. In adipocytes genes linked to protein and organelle turnover, branch chain amino acid catabolism, and lipolytic control were most significantly regulated. We identified a cell autonomous brake on adipocyte lipolysis via the neuropeptide Y receptor 1 (NPY1R). Expression of adipocyte *NPY1R* was reduced after weight loss and correlated positively with body fat percentage and body mass index. Findings were confirmed in meta-analysis across 23 studies. Finally, we found a negative correlation between *NPY1R* and beta-adrenergic-induced lipolysis and that NPY dose-dependently attenuated lipolysis and cAMP-signaling in primary human subcutaneous adipocytes.

**Conclusions:**

Our work suggests that decreases in adipocyte *NPY1R* during weight loss boost lipolytic capacity and contribute to improved systemic cardiometabolic health.

# Introduction

Despite the pharmacological breakthroughs for weight loss heralded by the GLP-1R agonists, obesity and its associated co-morbidities remain a global health crisis. Moreover, the current approved medications and most late-stage candidates in development focus mainly on appetite via neuronal pathways. Adipose tissues play a crucial role in cardiometabolic health through functions such as the safe storage and release of lipids, insulin sensitivity, and endocrine signaling [1]. Breakdown in these functions, as associated with obesity and lipodystrophies, is linked to dyslipidemia, insulin resistance, and type 2 diabetes (T2D) [2-6]. Notably, rescuing adipose tissue functionality, even without weight loss, in these pathological states is capable of reversing whole-body metabolic derangements, as evidenced by the Thiazolidinedione (TZD) class of T2D medications [2, 7]. Thus, collective clinical and genetic evidence [8-12] place adipose tissue at a pivotal tipping point on the scale dictating cardiometabolic health versus disease progression in obesity.

Adipose tissue is a key component in systemic lipid homeostasis through the regulated balance of uptake and lipolytic-driven release of fatty acids. Disrupting the lipolytic side of the axis has detrimental consequences [13] and leads to increased blood triglycerides and decreased HDL cholesterol levels [14]. A longitudinal clinical study from Arner and colleagues found that individuals who had lower expression of lipolysis-regulating genes in adipose tissue and inefficient lipolytic capacity gained more weight over a 13-year period [15]. Furthermore, the study reported that at baseline, individuals with high basal and low hormone-stimulated lipolysis were more predisposed for future development of insulin resistance [15]. Thus, understanding how adipose tissue biology and lipolytic dynamics can be modulated by different interventional contexts could help identify targetable approaches that improve long-term health following weight loss, sustain glucose and lipid homeostasis, and mitigate weight rebound.

# Results

## Mapping the impact of lifestyle intervention on adipose tissue with single cell resolution

The combination of reduced caloric intake and increased physical activity is a well-established paradigm for improving adipose tissue function and whole-body metabolic health [16-18]. Yet how such interventions impact the diverse cell populations comprising adipose depots remain largely unknown. Given the heterogeneity of adipose tissue [19, 20], we used single nuclei RNA sequencing (snRNAseq) to interrogate cell-specific changes in scWAT following a lifestyle intervention. We took advantage of a previous study, conducted by Bruun and colleagues in 2006 [17], in which scWAT biopsies were taken from 27 volunteers before and after 15-weeks of hypocaloric dieting (intake calculated to result in approx. 1% weight loss per week) and physical activity (2-3 hours of moderate intensity activity 5 times per week). We prepared nuclei and performed snRNAseq on frozen biopsies from 10 participants selected based on amount of material (n = 5 men and n = 5 women). Within this gender-balanced group, lifestyle intervention significantly improved several parameters of cardiometabolic health, including lowering BMI, waist circumference, fat percentage, blood leptin levels, increasing glucose tolerance and $VO_2$ max (**Figure 1A**). We mapped a total of 57,498 adipose nuclei from all participants samples before and after the intervention, with one exception where the RNA quality of one of the follow-up samples was too low to proceed with snRNAseq. The UMAP presented in **Figure 1B** contains an average of 3,026 ± 224 nuclei per sample (± standard error of the mean (SEM)) (min. 324 nuclei sample L "after" and max. 4,735 nuclei sample T "after"). The nuclei in the samples contain an average of 2,719 ± 118 gene per nuclei (± SEM) (min. 1,565 genes/nuclei sample B "before" and max. 3,498 genes/nuclei sample O "before").

These nuclei were grouped into 12 cell-class specific clusters, based on their expression of key marker genes described in previously published work on scRNAseq, snRNAseq, and spatial transcriptomics from adipose tissue (**Figure 1B and 1C**). The different cell types contributed at varying levels to the total number of cells in adipose tissue (**Figure 1D**). We profiled 10,144 nuclei from adipocytes (average of total cells: 17.8%, min: 7.7% , max: 26.6%), 18,632 adipocyte progenitor nuclei (average of total cells: 32.5%, min: 23.0% , max: 45.1%), 14,334 endothelial nuclei (average of total cells: 25.1%, min: 12.9% , max: 33.4%), 10,159 nuclei from immune cells

(average of total cells: 17,5%, min: 7,3% , max: 43,7%), 2,685 pericyte nuclei (average of total cells: 4.5%, min: 1.2% , max: 8.3%) and 1,655 nuclei isolated from smooth muscle cells (average of total cells: 2.6%, min: 0.1% , max: 9.6%). The cellular composition of each sample was similar between donors and between conditions. Over this relatively short intervention period, we did not observe significant changes in cell type fraction before and after lifestyle intervention (see **Supplementary figure 1**) and the overall distribution of nuclei in the different clusters were comparable to the snRNAseq atlas reported by Emont et al. 2022 [19] and Massier et al. 2023 [21].

## Differential expression analysis of adipose tissue after lifestyle intervention highlights control of adipocyte lipolysis

Differential expression analysis was performed on all cell-type clusters comparing before and after the intervention. Across all clusters, we identified 10,794 differentially expressed genes (DEG) (adjusted p-value < 0.05) (**Figure 2**), amongst these we found 2,471 genes that were significantly decreased after intervention (adjusted p-value < 0.05, and average $\log_2$ fold change < 0) and identified 8,323 genes that were significantly increased by the lifestyle intervention (adjusted p-value < 0.05, and average $\log_2$ foldchange > 0) (**Figure 2**). These snRNAseq findings reveal robust changes within the adipose tissue following lifestyle intervention with cellular resolution. We identified DEG in all cell-type clusters (**Figure 2**, gene list **Supplementary data in excel file**), demonstrating that the lifestyle intervention broadly impacts the heterogenous cell populations within adipose tissue. In particular, the high number of detected genes in the macrophage populations could be indicative of a functional shift between the cells inside the cluster that signifies a change in inflammatory status (**Figure 2**). This provides an improved high-resolution understanding of the original observations from this cohort [17]. Interestingly, we detected relatively few DEG from the arteriolar endothelial cells compared to the other endothelial cell populations, suggesting that any alterations in vessel function might be driven more by changes on the nonarterial side of the vascular network (**Figure 2**).

The cell-type with the most DEG was adipocytes with a total of 4,920 identified genes. Of these, 4,612 genes displayed increased expression (**Supplementary data in excel file**), whereas 388 genes were downregulated (**Supplementary data in excel file**). Using DAVID functional annotation analysis, we then identified KEGG pathways that were significantly differentially regulated (**Table 1**). KEGG analysis of the intervention-induced genes successfully mapped 1,901 of the uploaded genes, representing 41.8% of the total gene list, and resulted in 118 identified

pathways (**Table 1**). The top upregulated pathway "Autophagy - animal" (hsa04140) along with the tenth most significantly increased pathway "Mitophagy - animal" (hsa04137) suggested a potential increased turnover in cells following weight loss. The second and fifth most upregulated pathways "Valine, leucine, and isoleucine degradation" (hsa00280) and "Propanoate metabolism" (hsa00640) both support catabolism of branch chain amino acids (BCAAs). BCAAs are among the metabolites most strongly positively correlated with insulin resistance and type 2 diabetes [22]. Therefore, our snRNAseq findings of a significant increase in genes linked to BCAA breakdown, together with the observed induction of the "Insulin signaling pathway" (hsa04910) (i.e. the seventh most induced pathway), collectively support a mechanism through which the adipose tissue could contribute to the improved glucose control, reported in the original study [17].

In the analysis of the genes with decreased expression after lifestyle intervention (**Supplementary data in excel file**), we identified and successfully mapped 189 unique genes (49.0% of the total uploaded genes) to KEGG pathways (**Table 1**). The most downregulated pathway following the diet and exercise-based intervention was the "Regulation of lipolysis in adipocytes" (hsa04923), which in combination with the downregulation of genes linked to "Insulin Resistance" (hsa04931) also supports improved glucose homeostasis. The pathway "Regulation of lipolysis in adipocytes" was based on the intervention-suppressed expression of 7 genes, *INSR*, *NPY1R*, *AQP7*, *ADCY6*, *GNAI1*, *MGLL*, and *PNPLA2*. Interestingly, neuropeptide Y receptor 1 (NPY1R) is a $G_i$-coupled receptor that has been reported to inhibit adenylate cyclase through the G protein subunit alpha i1 (GNAI1) [23]. The significant decrease in both *NPY1R* and *GNAI1* suggests that downregulation of *NPY1R* signaling in adipocytes could be important for intervention-mediated improvements.

## An NPY-NPY1R signaling axis in human subcutaneous adipocytes

Recent work has functionally linked *NPY1R* to mural cells in mouse thermogenic adipose tissue [24]. While its expression has also been reported in human scWAT [25, 26] , the cell-specific distribution of *NPY1R* expression in human adipose depots remains unresolved. Our snRNAseq findings demonstrate that *NPY1R* levels are most robustly enriched in the mature adipocyte and smooth muscle cell population (**Figure 3A)**. Moreover, this is consistent with earlier profiling of scWAT [19, 25, 26]. *NPY1R* is the predominant family member expressed in adipose tissue as we could not detect *NPY2R* mRNA and both *NPY4R* and *NPY5R* displayed very low expression across all cell-types (**Figure 3B**). We also did not detect any significant expression of ligands for this family of receptors, including neuropeptide Y (*NPY*), peptide YY (*PYY*) or pancreatic polypeptide

(*PPY*) (**Figure 3B)**. This suggests that the source of the neuropeptide ligand for NPY1R comes from outside the tissue or via neurons, rendering single cell or nuclei RNAseq approaches to study scWAT unable to capture mRNA expression of the ligand. An analogous paradigm was recently reported for oxytocin receptor signaling in adipose tissue [27]. Thus, our findings show that *NPY1R* expression is highly specific for adipocytes and smooth muscle cells.

NPY1R can be activated by full-length NPY or PYY but not PPY. NPY1R requires the N-terminal residues of the ligands and, therefore, is not fully activated by truncated NPY or PYY (3-36) [28, 29]. Consequently, given that the majority of circulating PYY is truncated by tissue-resident peptidase, DPP4, to PYY 3-36 [30], the predominant *in vivo* ligand for NPY1R is NPY. NPY4R is activated predominantly by PPY with some activity from NPY and NPY5R can be activated by NPY, PYY, and NPY 3-36 [31, 32]. However, the relatively low expression of both NPY4R and NPY5R in scWAT cell populations suggests that these receptors are not playing a direct role in tissue function. To that end, we did detect full-length amidated NPY in human adipose tissue using a separate, independent donor cohort (**Figure 3C**) interestingly NPY has also been detected in mouse epididymal and subcutaneous fat [33]. Conversely, we were unable to detect PPY or PYY at the protein level in adipose tissue biopsies, supporting the model whereby NPY-NPY1R is the primary signaling axis in human scWAT.

Earlier studies demonstrated that NPY is co-transmitted with norepinephrine (NE) from noradrenergic neurons [34, 35]. Perivascular and parenchymal NPY-containing sympathetic neurons have been reported in white adipose tissue of rats [36, 37]. Using a double staining approach to image *NPY1R* mRNA and protein gene product 9.5 (PGP9.5), a highly specific neuronal marker [38], we identified parenchymal expression of *NPY1R* mRNA in close proximity to PGP9.5 (**Figure 4A** and close-up **Figure 4B**). Signal specificity was assessed in the perivascular neurons, by performing double staining, substituting *NPY1R* mRNA with Rhodopsin mRNA in the presence of PGP9.5. For PGP9.5, we verified signal specificity by omission of antibody and with an isotype control (**Figure 4C-F & J**). *NPY1R* mRNA expression was located inside and in close proximity to nuclei of cells staining positive for Perilipin 1 (PLIN1), an adipocyte marker (**Figure 4G**) [21], whereas PGP9.5 was dispersed in the parenchyma of the tissue located around the PLIN1-positive cells (**Figure 4H**). PGP9.5 signal was also detected in perivascular neurons (**Figure 4I**). The histological examination of *NPY1R* mRNA demonstrates that *NPY1R* is expressed by adipocytes in close proximity to PGP9.5-positive neurons (**Figure 4B**). Taken

together, our data show an NPY-*NPY1R* paracrine signaling axis between neurons and human subcutaneous adipocytes.

## Clinical correlation of *NPY1R* in human adipose tissue during weight loss

To further interrogate the potential clinical relevance of *NPY1R* in scWAT, we investigated spearman correlations of *NPY1R* mRNA with the metadata from the original study by Bruun et al. 2006 [17]. In the adipocyte cluster from the snRNAseq (from **Figure 1A**), *NPY1R* mRNA levels were positively correlated with BMI (linear regression analysis $R^2 = 0.2139$, p-value = 0.0462, **Figure 5A**), body fat percentage (linear regression analysis $R^2 = 0.4463$, p-value = 0.0018, **Figure 5B**), and waist circumference (linear regression analysis $R^2 = 0.2850$, p-value = 0.0186, **Figure 5C**). In the data we also found a significant correlation between *NPY1R* mRNA and leptin levels (linear regression analysis $R^2 = 0.2460$, p-value = 0.0429, **Figure 5D**), which could suggest a direct coupling to adipocyte function. Collectively, these correlations between *NPY1R* and various clinical biometric parameters are consistent with the observed downregulation of *NPY1R* following lifestyle intervention-induced weight loss.

In order to further investigate the involvement of adipose tissue *NPY1R* in cardiometabolic health we sought to the evaluate our findings across 23 independent studies compiled on the Adipose Tissue Knowledge Portal (ATKP, adiposetissue.org) [39]. Using the ATKP, we found that *NPY1R* expression levels were significantly reduced following bariatric surgery and dietary intervention (**Figure 5E**), supporting our findings from lifestyle intervention. Moreover, we confirmed the clinical correlations to BMI, waist circumference, and WAT LEP secretion, as well as several new associations, including circulating insulin and HOMA-IR (**Figure 5F-I**). The ATKP further showed that *NPY1R* mRNA expression is positively associated with fat cell volume (**Figure 5J**) and negatively correlated with isoproterenol-induced lipolysis (**Figure 5K**), suggesting that NPY1R signaling has a negative effect on release of free fatty acids from adipocytes [15, 39-60]. This is in line with NPY1R being a $G_i$-coupled receptor that inhibits cAMP production and thereby lipolysis activation.

Next, we functionally assessed the effects of NPY on isolated mature human subcutaneous white adipocytes. We found that NPY effectively reduced isoproterenol-induced lipolysis in freshly isolated adipocytes from 3 different donors (**Figure 6A-C**). These findings were confirmed in 3D culture by measuring the relative cAMP levels following 1 hour of stimulation with isoproterenol

in the presence or absence of NPY co-administration (**Figure 6D-G**). The measurements on cultured adipocytes were done using material from four different donors. Our analysis demonstrates that NPY causes a dose-dependent decrease in inducible lipolysis and cAMP signaling in human adipocytes. These data are consistent with earlier studies on immortalized murine white adipocytes [61, 62] and ex vivo human scWAT biopsies [63, 64].

Thus, our collective findings reveal that NPY-NPY1R signaling in human white subcutaneous white adipocytes attenuates beta-adrenergic responsiveness. This paracrine axis is elevated under obesogenic conditions and reduced after lifestyle intervention-mediated weight loss, making it an appealing target for exploring pharmacological approaches that antagonize adipocyte NPY1R for cardiometabolic health.

# Discussion

Our data represents the first snRNAseq map resolving how a diet and exercise weight loss regimen shapes the cellular landscape of human adipose tissue. The pathways we found regulated in adipocytes suggest an adaptive biological change that improves responsiveness to external lipolytic signals. In our studies, we measured a comparable distribution of nuclei across cell types before and after the lifestyle intervention, consistent with previously reported snRNAseq analyses of human adipose tissue [19]. However, a recent study by Miranda et al. [65], in which snRNAseq was performed on scWAT before and after bariatric surgery-induced weight loss, detected major shifts in cell populations. In our study these shifts were not detected, which is likely due the difference in timing between the two studies: the study we analyzed, from Bruun et al. [17], was a 15-week lifestyle intervention whereas Miranda et al. [65] collected samples a minimum of 5-months post bariatric surgery (median 7, range 5–18 months). This could also explain their discovery that long-term weight loss rescues cellular senescence whereas our more acute findings uncovered changes in lipolytic control. Also, the subjects in the present trial are younger on average than the ones analyzed in Miranda et al. Age is known to have a profound effect on the cellular composition, especially with respect to immune cells in adipose tissue [66]. In addition, the obtained weight loss varied between the studies, in Miranda et al the median percentage weight loss was 22% (range 13–33%) [65], whereas the weight loss was lower in this subset of Bruun et al. median percentage WL was 12% (range 4-18%) [17].

Notably, our use of decades-old bio-banked material also highlights the feasibility and opportunity to retroactively interrogate adipose tissue samples from older, well-characterized cohorts. Our

FACS-free protocol makes it possible to use samples that have been under long-term storage for snRNAseq analysis. The depth of resolution of the single cell transcriptomes also allows contextualization of earlier findings and interpretations. For example, the original clinical study reported a reduction in adipose tissue macrophage infiltration, as assessed by measurement of *CD68* and *CD14* mRNA levels, which correlated with reduced whole-body inflammation [17]. However, accounting for larger sets of transcriptomes instead of select genes, we could not detect any clear difference in cellular population induced by the lifestyle intervention. This might suggest that while resident macrophages undergo significant adaptation in inflammatory profile during weight loss, the absolute cell number remains unchanged. Alternatively, population changes might be driven by expression patterns in a small number of genes and/or in a subset of cells within the specific clusters. A more fine-tuned approach to analyzing the cell clusters is needed to uncover potential cellular trajectories underlying shifts in these sub-populations.

Most strikingly, our snRNAseq data indicate that NPY1R is the predominant NPY receptor in human scWAT. We found that *NPY1R* expression in human adipocytes correlates with BMI (**Figure 5A & G**) and has an inhibitory effect on lipolysis in isolated human adipocytes and on cAMP in 3D cultured adipocytes (**Figure 6**). These findings, supported by previous studies Serradeil-Le Gal et al. 2000 [26], suggest that NPY activates adipocyte NPY1R to control lipolysis in humans. High levels of *NPY1R* in human adipocytes are also observed in the data available from Emont et al. 2022 [19] and Miranda et al. 2025 [65]. Extracting adipocyte *NPY1R* expression from the latter dataset further revealed substantially increased levels in the adipocytes of the obese subset compared to the levels in lean individuals (see **Supplementary figure 2**) [65]. Interestingly, the presence of *NPY1R* on white adipocytes appears to be a human phenomenon. Using the publicly available data from Emont et al. 2022 [19], high levels of *NPY1R* were detected in human but not mouse adipocytes. This species difference adds a layer of complexity to the role of NPY1R in adipose tissue. Indeed, a recent report from Zhu et al. 2024 [24] found that, in mice, activation of NPY1R in mural cells was critical for sustaining the murine thermogenic adipocyte population and promoting energy expenditure.

In accordance with our findings, earlier studies reported that baseline *NPY1R* expression level was predictive for a transcriptome profiling-based model of weight maintenance, Armenise et al. 2017 [50]. In the model *NPY1R* is one of multiple parameters including other gene levels and anthropometric markers. Furthermore, Armenise et al. 2017 [50] found a reduction in *NPY1R* levels following low caloric diet. Additionally Feng et al. 2022 [67], showed that *NPY1R* was

significantly higher expressed in adipose tissue of children with obesity compared to children without obesity and. Hua et al. 2023 [68], found that *NPY1R* expression is increased in adipose tissue in obesity. Our findings along with the collective data reported by these three studies show that adipose tissue *NPY1R* expression increases with the development of obesity (**Figure 5**) and correlates positively with bodyweight. While the cause of bodyweight driven increase in *NPY1R* expression remains to be determined, our data showing that NPY1R signaling interferes with β-adrenergic signaling and induction of lipolysis in human adipocytes, implicates NPY1R in the obesity-driven cell autonomous disruption of lipolytic plasticity. In our study, the sensitivity to both isoproterenol and to NPY varied between donors. Due to the relatively few donors, we were unable to identify underlying mechanisms for this donor variation in the present study. However, future studies interrogating the degree of variability on a larger scale could provide a more comprehensive picture of the role of adipose tissue NPY-NPY1R signaling in controlling lipid release and possibly even affecting the development of obesity. Nevertheless, even in our smaller scale study, the fact that a reduced ability to stimulate lipolysis is linked to weight gain and deteriorated glucose tolerance [23] place adipocyte NPY1R in a potentially critical axis for cardiometabolic health.

We further show, through histological examination of *NPY1R* mRNA, that NPY1R is expressed by adipocytes in proximity to $PGP9.5^{+}$ neurons. In a recent study, Willows et al. 2021 [69] visualized $PGP9.5^{+}$ neurons in whole-mounted adipose tissue from mice, and identified nerve terminals surrounding adipocytes that they denoted as the neuro-adipose nexus. While the present data lacks three dimensionality, the *NPY1R* mRNA and PGP9.5 stain (**Figure 4B**) are consistent with a similar neuro-adipose nexus in human scWAT. Alternatively, the proximity of *NPY1R*-expressing adipocytes to $PGP9.5^{+}$ neurons could be indicative of paracrine signaling via neuronal varicosities in addition to or instead of nerve terminals. NPY and beta-adrenergic agonist, NE, are co-released from sympathetic neurons [70]. Therefore, the increased expression of NPY1R in adipocytes during obesity likely serves as a pathological brake on neuronal stimulation of adipose tissue metabolism and here we show that one of the benefits of lifestyle interventions involving diet and exercise is to reduce *NPY1R* in human scWAT. Further characterization of the human NPY-NPY1R axis, including how it is regulated in response to increased adiposity, could represent a novel, targetable means of correcting lipid metabolism and glucose control, reducing adipose tissue mass, and improving overall health outcomes.

# Ethics

## Samples from Bruun et al. 2006

For the study of Bruun et al. 2006 [17], informed, written consent was obtained from all subjects, and experiments were performed in accordance with the Helsinki II Declaration. The study was approved by the Ethical Committee of Copenhagen (KF 01-220/03). In compliance with current regulations on General Data Protection Regulation (GDPR), the current project was registered and granted approval by The Danish Data Protection Council. All personal data were handled in accordance with EU Regulation 2016/679, on the protection of natural persons with regard to the processing of personal data and on the free movement of such data.

## Samples from Genoskin

Human samples of abdominal subcutaneous adipose tissue were purchased from the European Genoskin site (Toulouse, France). All donors were volunteering adults who undergo surgery and received written and oral information before signing an Informed Consent form to donate the residual skin (including adipose tissue) that would otherwise be destroyed. Informed, written consent was obtained from all subjects, and experiments were performed in accordance with the Helsinki II Declaration. Genoskin has all legal authorizations necessary from the French Government and the appropriate Ethics Committee. Genoskin has Biological Sample Transfer Agreements with several French hospitals and clinics, in order to comply with all applicable regulations for the retrieval and use of human skin tissue for research purposes. For more information about Informed Consent, and Biological Sample Transfer Agreements please consult Genoskin website, link in reference [71] and [72].

## Samples for the peptide enrichment analysis.

For peptide enrichment analysis ten healthy men were recruited for the study. The study was approved by the Copenhagen Ethics Committee (Reg. number H-16040740) and performed in accordance with the Declaration of Helsinki. Informed written consent was received from each participant prior to study inclusion. All subjects were healthy, moderately physically active and with no family history of diabetes. The subjects were 27 ± 0.8 (means ± SEM) years old, with a body weight of 85 ± 2.5 kg, body mass index (BMI) of 24 ± 0.5 kg/$m^2$.

# Material and methods

## Adipose tissue biopsies

The human samples were originally collected in the study of Bruun et al. 2006 [17]. Briefly the participants were recruited from Ebeltoft Kurcenter and the original open study included 27 participants. However, due to limited material 10 of these participants were included in the present study. The 10 participants represented in this study were severely obese at project start with a mean BMI of 46.0 ± 3.1 kg/m$^2$ and a BMI range of 31.4–63.0 kg/m$^2$, with a 50/50 female/male ratio. After intervention mean BMI was 40.8 ± 2.8 kg/m$^2$ with BMI range: 27.4–57.5 kg/m$^2$. These participants took part in 15-weeks of consecutive lifestyle intervention consisting of a hypocaloric diet and moderate physical activity. Hypocaloric diet was calculated for the specific participant and calculated to reduce the subject's body weight by approximately 1% per week. The exercise consisted of 2-3 hours of moderate-intensity physical activity (e.g. walking or swimming) 5 days per week. The specific details are reported in Bruun et al. 2006 [17].

In the study, body composition was assessed by bioelectric impedance (Quantum X; RJL Systems), and the waist circumference was measured at the midpoint between the upper iliac crest and lower thoracic rib at the level of the umbilicus [17].

Data and human samples were collected before (baseline) and repeated after the 15-weeks of lifestyle intervention. At least 6 hours before sampling the subjects were fasting and had not engaged in vigorous physical activity. Fasting and inactivity periods were standardized between baseline and after intervention. Adipose tissue samples were obtained from the subcutaneous abdominal depots as described in a previous study [73]. Briefly the skin was anesthetized with lidocaine (10 mg/mL), before a small incision was made and a minimum of 200 mg of adipose tissue was removed under sterile conditions. Immediately after removal the adipose tissue was washed with isotonic NaCl, snap-frozen in liquid nitrogen and kept at -80 °C. Some of the material was removed and used for RNA extraction in the original study [17]. Furthermore, the material has contributed to other additional studies, Bruun et al. 2007 [74], Helge et al. 2011 [75] and Kristensen et al. 2017 [76]. The remaining material was stored in a temperature monitored -80 °C freezer until the start of this present study.

## Isolation of mature human adipocytes

Isolation of human adipocytes was done from large quantities of human subcutaneous adipose tissue. For this purpose we received samples of minimum 100 g, collected by Genoskin from volunteering patients who are undergoing surgical intervention, such as abdominoplasty. Tissue was processed in pieces of approximately 10 g. Adipose tissue was removed from the connective tissue and larger blood vessel by gently scraping the tissue with the back of a closed scissor. The larger blood vessels and connective tissue were discarded after scraping, and the remaining tissue was minced using a scissor. The processing was repeated until all tissue was processed. The minced tissue was transferred to 50 mL conical tubes, transferring approximately 10 mL tissue to each tube, and 30 mL Degradation buffer (see **Supplementary Table 1+2**) was added to each tube. The tubes were then incubated at 37 °C in a shaking incubator at 130 rpm, with an average incubation time of 45 minutes. Incubation time slightly varied due to visual inspection of degradation levels every 5 minutes after the 20-minute mark. Digested tissue was then filtered through 2 layers of sterile gaze, and transferred to new 50 mL tubes, with addition of 20 mL wash buffer (see **Supplementary Table 1+2**) to stop the degradation. After a few minutes the buoyant adipocytes float to the top, separating from the Stromal Vascular Fraction (SVF), as described by Rodbell 1964 [77]. The SVF and wash buffer were removed using a syringe, and the washing was repeated two additional times, discarding the infranatant each time. Adipocytes were then spun at 10 x g for 30 seconds to increase the final concentration the remaining wash buffer was removed using a syringe, resulting in 40-70 mL of highly concentrated adipocyte suspension (close to 100% adipocytes). The protocol described above was based on the protocol by Rodbell 1964 [77] and modified as described Harms et al. 2019 [78], and the video version [79], with further optimization in our laboratory.

## Measuring release of fatty acids

Isolated mature human adipocytes (close to 100% adipocytes) were resuspended and diluted in Lipolysis Buffer (see **Supplementary Table 1+2)** to approximately 25% (v/v) adipocyte concentration in a 96-well plate (Clear Flat-Bottom Immuno Nonsterile 96-Well Plates MaxiSorp, Thermo Scientific cat. 439454). Titration curves with varying doses of ISO or NPY at fixed ISO concentration were dissolved in 100 µL Lipolysis Buffer. Adipocytes were stimulated with varying concentration of Isoproterenol (ISO) or a fixed ISO dose with varying NPY concentration (recombinant full-length human NPY produced at Novo Nordisk) for 1 hour at 37 °C on a plate-shaker at 400 rpm. 40 µL of media or standard curve dilution (Wako NEFA St.

solution stock 1mM) was transferred to a new plate and fatty acids in the media were measured using NEFA-HR(2) Assay (FUJIFILM Wako Chemicals). To the 50 µL stimulated media 50 µL NEFA-HR(2)R1 was added, plates were incubated for 10 minutes at 37 °C with shaking at 400 rpm. 25 µL NEFA-HR(2)R2 was added and plates were incubated for 10 minutes at 37 °C. The colorimetric assay was measured as optical density at 560 nm on Sunrise absorbance reader (Tecan). Interpolated values were reported as means of technical duplicates for each sample with error bars representing SEM.

## Encapsulation in HyStem-C Cell Culture Scaffold

Adipocytes were encapsulated into HyStem-C, a Thiol-Modified Hyaluronan and Gelatin Hydrogel (Advanced Biomatrix, cat. no. GS313F). Consisting of thiol-modified hyaluronan (Glycosil), thiol-reactive crosslinker, PEGDA (Extralink), and thiol-modified denatured collagen (Gelin-S). The vials were reconstituted as per manufacturer's instructions, in a 37 °C oven (atmospheric $CO_2$). Glycosil and Gelin-S were mixed in 1:1 ratio. The required volume (40 µl/well in 96-well format) of highly concentrated adipocytes (close to 100% adipocytes) were placed in a separate tube, and any residual wash buffer was removed. 20 µL/well Glycosil:Gelin-S mixture was added to the adipocytes resulting in an adipocyte concentration of 50-66% (v/v). For 96-well plates 20 µL/well adipoicyte:Glycosil:Gelin-S mixture was added and 5 µL Extralink. Following addition of Extralink, plates were gently shaken from side-to-side to mix the components. Plates were incubated in an oven at 37 °C (atmospheric $CO_2$) for 60-90 minutes. After 10 minutes plates were heavily shaken to ensure adequate mixing and gelation, and gelation was assessed after 45 minutes. After gelation 150 µL Adipocyte Culture media (see **Supplementary Table 1+2**) was added. The cells were then incubated in an incubator at 37 °C, 5% $CO_2$, for approximately a week before usage, with daily media changes. The HyStem-C hydrogel has previously been used for human adipocytes in a Tissue-on-Chip culture by Rogal et al. 2022 [80], and for static 3D culture by Hong et al. 2014 [81].

## Measuring cAMP levels

HyStem-C adipocytes cultured in 96-well format were washed with DPBS, and cAMP starvation buffer (see **Supplementary Table 1+2**) was added. Adipocytes were then incubated for 1-2 hours at 37 °C, 5% $CO_2$ before stimulation. Following starvation adipocytes were stimulated with varying concentration of ISO or a fixed ISO dose with varying NPY concentration

(recombinant full-length human NPY produced at Novo Nordisk). Adipocytes were stimulated in cAMP Assay buffer (see **Supplementary Table 1+2**) for 1 hour at 37 °C and 400 rpm shaking. Adipocytes were lysed using Lysis & Detection buffer from cAMP Gs dynamic kit (Revvity, cat. no. 62AM4PEC) and vigorously mixed by pipetting up and down. Lysate was then incubated for 15 minutes at 37 °C and 400 rpm shaking. 10 µL of sample was transferred from each well carefully avoiding the floating lipids. The continued analysis was run using cAMP Gs dynamic kit (Revvity, cat. no. 62AM4PEC) according to manufacturer's instructions, including dilution of standard. Plates were read on a Mithras Microplate reader (Berthold Technologies). HTRF ratio was measured and calculated by the Mithras (fluorescence ratio = (Signal 665 nm / Signal 620 nm) * 10.000). cAMP levels were calculated from the diluted standard as described by the manufacturer. Interpolated values were reported as the means of technical duplicates for each sample with error bars representing SEM.

## Nuclei isolation and counting

Nuclei were isolated using a modified version of the Nuclei Isolation Kit: Nuclei PURE Prep (Sigma-Aldrich, cat. no. NUC201). The entire protocol was carried out on ice, and the protocol used on average ~233 mg of adipose tissue (lowest amount was 200 mg and highest 270 mg), which yielded an average 175,000 nuclei per sample in 200 µL (lowest 66,800 nuclei and highest 254,000 nuclei). The tissue was lysed in 2 mL ice cold Nuclei Lysis Buffer (see **Supplementary Table 1+2**). Briefly chopped into pieces with a scalpel and homogenized for 30 sec at 20,000 rpm using an ULTRA-TURRAK TP18/10 homogenizer. The homogenized tissue was then lysed for 10 minutes, filtered through a 40 µm cell strainer and collected in Eppendorf DNA LoBind tubes. The nuclei were then pelleted by centrifugation at 500 x g for 10 min at 4°C. Following centrifugation, the supernatant was carefully removed, and the pellet was resuspended in Nuclei Wash Buffer (see **Supplementary Table 1+2**). The process of filtering, centrifugation and resuspending was repeated once, followed by a wash without filtering for a total of three washes. The lysate was then mixed with 1.8 M Sucrose Cushion Solution (see **Supplementary Table 1+2**) resulting to a sucrose solution of ~1.16 M Sucrose. The mixture was then carefully loaded on top of 500 µL 1.8 M Sucrose Cushion Solution, and centrifuged at 13,000 x g, at 4°C for 45 min. The supernatant was then carefully removed, and the nuclei pellet was resuspended in wash buffer, centrifuged at 500 x g for 10 min at 4°C, resuspended in wash buffer, and filtered once more through a 40 µm filter. Finally, the pellet was resuspended in ~200 µL of wash buffer and

counted using NucleoCounter NC-200 (ChemoMetec) to determine nuclei concentration. Protocol was loosely based on Martelotto 2020 “Frankenstein” protocol [82].

## Single nuclei RNAseq using Chromium Next GEM Single Cell

For isolation of single nuclei RNA, the samples were run using the 10x Genomics Chromium Next GEM Single Cell 3′ Reagent Kits v3.1 on a 10x Chromium Controller according to manufacture’s instructions (protocol version “CG000204_ChromiumNextGEMSingleCell3_v3.1_Rev_D”). Before loading the samples, the nuclei were diluted to be below 1200 nuclei/µL. The average loading concentration was ~875 nuclei/µL after dilution (min. 128 nuclei/µL max. 12,700 nuclei/µL) and ~8300 nuclei were loaded from each sample for an expected recovery of up to 5000 nuclei/sample. During the run, the sample cDNA quality control and quantification was assessed using Bioanalyzer High Sensitivity DNA kit (Agilent). The samples were assigned unique sample index sequence sets from the Dual Index Kit TT Set A 96 rxns plate, (10x Genomics). Post run the Agilent Bioanalyzer High Sensitivity DNA kit was used to estimate fragment size, coupled with a concentration measurement on a Qubit 4 Fluorometer (Invitrogen) using the Qubit 1X dsDNA HS Assay Kit (Invitrogen). The sample libraries were diluted to the same concentration 5 nM dsDNA libraries and were pooled to a single balanced library before sequencing.

## NovaSeq 6000 sequencing

The libraries were sequenced on an Illumina NovaSeq 6000 sequencing system and run using the NovaSeq 6000 S4 Reagent Kit v1.5 (200 cycles) (Illumina). With potentially 16–20 billion Paired-end Reads passing filter. This results in a sequencing depth of up to approx. 100.000 reads per nucleus. The pooled library with nuclei isolated from 20 samples were loaded onto a single chip and spiked with 1% PhiX (Illumina). The NovaSeq 6000 was run according to the manufacturer’s instructions, with sequencing run set to as described in (“CG000204_ChromiumNextGEMSingleCell3_v3.1_Rev_D”).Briefly, we used paired-end, single indexing with the following cycle settings: Read 1 at 28 cycles (10x Index and UMI), 8 cycles (i7 Index), 0 cycles (i5 Index) and Read 2 at 91 cycles.

## Single-nucleus RNA-seq analysis

BCL files were demultiplexed into FASTQ files using Cellranger mkfastq software (v6.1.1) [83].

Salmon Alevin v1.4.0 [84] and Alevin-fry v0.3.0 [85] were used to perform pseudoalignment of the FASTQ files to a customized GRCh38 genome (assembly GCF_000001405.26) [86], modified into discriminating between mature mRNA and pre-mRNA using the *make_splici_txome* function from alevin-fry-tutorials [87]. Cell calling was done on the unfiltered count matrix with *barcodeRanks* function from the *DropletUtils* package [88-90]. Ensembl gene IDs were mapped to symbol with the *mapIds* function from the *AnnotationDbi* package [91]. The Seurat objects were converted to a singleCellExperiment object. RNA counts were log-normalized and PCA was performed. An individual doublet score for each cell was then computed with the *computeDoubletDensity* function from the *scDblFinder* package [92, 93]. After processing the individual sequence reactions, all results were aggregated into a single object. All individual reactions were filtered for common genes between them and then merged. Genes without any detection in the merged objects were then removed, and all blacklisted cells were removed. The object was then normalized using *SCTransform* [94], and PCA was performed. The Global dimensions were calculated using *maxLikGlobalDimEst* function from the *intrinsicDimension* library [95]. Using the Seurat (v4) package we ran *RunUMAP*, *DimPlot*, *FindNeighbors*, and *FindClusters* functions (using the Leiden algorithm [96]) [97]. The resulting data was saved as a filtered object containing the filtered RNA and SCT assays. The continued analysis was run on the SCT assays. Upon analyzing the data, two clusters were removed that likely represented doublets, due to the presence of multiple key marker genes

## Cluster identification

Cluster identification was run at multiple Leiden Resolutions (0.3 to 0.8) resulting in a maximum of 22 separate clusters. These clusters were reduced by combining clusters of the same cell types in order to increase the number of cells per cluster and to ensure that genes identified were robustly expressed in the given cell types.

Clusters were manually annotated using markers from previously published work on scRNAseq, snRNAseq and spatial transcriptomics [19, 21, 98-102]. The following marker genes were used to identify the different clusters based on previous publications (**Figure 1C**): adipocytes were defined as expression of *ADIPOQ, PLIN1* and *PLIN4*, in accordance with [19, 98]. Adipocyte progenitor cells were defined by *PDGFRA* and *LUM* expression, [19, 98, 102]. Endothelial cells were defined by expression of marker genes *VWF* and *PECAM1*, [98, 102]. Endothelial cells were subdivided into endothelial cells from artery and/or arterioles, by expression of *SOX17* [21],endothelial cells from the microvascular by expression of *RBP7* [99], endothelial cells from

veins and/or venules, by expression of *SELP* [21] and endothelial cells from lymphatic vessels, by expression of *MMRN1* [103, 104]. Immune cells were identified by expression of hematopoietic marker *PTPRC* (*CD45*) [99]. In this branch of clusters, we identified macrophage by expression of *CD163* [100]. Furthermore, we identified lymphocytes by the expression of *CD96* [103]. Mast cells were identified by the expression of *KIT* [105]. We identified a population of pericytes by the expression of *PDGFRB* and smooth muscle cells by the expression of *MYH11* [19, 98, 102].

At Leiden Resolution 0.8 the identified clusters contain additional subclusters. Adipocyte progenitor separates into 6 subclusters. Adipocytes are separated into 4 subclusters. Dendritic Cells is 1 cluster. Endothelial cells separate into the 4 clusters presented in the UMAP (**Figure 1B**). Lymphocyte is 1 cluster. Macrophage separate into 2 subclusters. Mast cell is 1 cluster. Pericyte is 1 cluster. Smooth Muscle cell is 1 cluster.

## Differential expression analysis

Differential expression analysis was done by comparing the expression value "before" intervention with "after" intervention on the 12 cell clusters. Differential expression was done using *rank_gene_groups* from the Scanpy package (version 1.9.6) [106] comparing the gene expression between the samples from the "before" and "after", using non-parametric Wilcoxon rank sum test. Adjusted p-value, were Bonferroni-corrected across all features [97].

Functional analyses were done using the "DAVID 2021 (Dec. 2021), DAVID Knowledgebase (v2023q4, updated quarterly)" [107, 108]. Genes identified as significantly regulated (adjusted p-value < 0.05) from the differentially expressed gene analysis of the adipocyte cluster, were uploaded as gene list, to the DAVID platform and analyzed using the KEGG pathway tool, using "Official Gene ID's and the Homo sapiens gene from DAVID as reference. Gene lists were separately uploaded for up and down regulated genes (defined as a positive or negative average $\log_2$ fold change). The resulting list was then reduced to only include pathways with a p-value < 0.05.

## Peptide enrichment

Human subcutaneous abdominal adipose were collected by needle biopsy (approx.150 mg) under local anesthesia with 1% lidocaine from 10 healthy men in the age between 25-35 years with a BMI ≤ 25. Fat biopsies were rinsed in ice-cold saline and frozen in liquid nitrogen and stored at -80°C. For analysis, the fat biopsies were taken directly from a frozen state and heated to 95 °C in

an air-evacuated cartridge in a Denator T1 heat stabilizor [109]. Extraction of peptides was done essentially as [110] with the following modifications. We used 5 µL/mg tissue weight of 0.5% acetic acid. Microcon YM-10 cut-off filters (Millipore) were preconditioned with 500 µL 2% MeCN/3% MeOH and 500 µL 5 M urea in 0.5% acetic acid. The filtrate was pooled and fractionated by strong cation exchange (SCX). SCX fractionation was done using an in-house STAGE tip packed with six SCX disks (Em-pore SPE Disks #66889-U). The SCX-tips were equilibrated 100 µL of buffer 0.5% acetic acid, 20% acetonitrile. Peptides were eluted into ten (10) SCX-fractions (pH 4; 4.5; 5.0; 5.5; 6.0; 6.5; 7.5; 9.0 11.0 and FT). Each SCX fraction was then loaded onto in-house packed reverse-phase C8 STAGE tips with two Empore C8 discs preconditioned with 40 µL MeOH, 40 µL 80% MeCN/0.5% acetic acid and twice with 50 µL 0.5% acetic acid/0.1% trifluoroacetic acid (TFA). Stage tips were washed twice with 200 µL 0.5% acetic acid/0.1% TFA. The peptides were eluted from the C8 STAGE tips into a 96-well microtiter plate with 40 µL of 40% acetonitrile (ACN), 0.1% formic acid and 60% ACN 0.1% formic acid, respectively in the same sample well. The samples are now ready for LC-MS analysis.

## Mass spectrometry analysis

The peptides were eluted from the C8 STAGE tips into a 96-well microtiter plate with 40 µL of 40% acetonitrile, 0.1% formic acid and 60% ACN 0.1% formic acid, respectively. Peptides were reconstituted in 10 µL 2% MeCN, 0.5% acetic acid, 0.1% TFA after vacuum centrifugation in a speed-vac. 5 µL of the peptide eluate was separated by a 120 min gradient using a 15-cm fused-silica emitter packed with reversed-phase ReproSil-Pur C18-AQ 1.9 µm resin (Dr. Maisch GmbH) using a nanoflow Easy-nLC system (Thermo Scientific). The MS analysis was done using a QExactive HF orbitrap instrument, and the samples were analyzed using a top-10 higher-energy collisional dissociation (HCD) fragmentation method [111].

## Peptide identification and search

Raw files were processed using MaxQuant (v1.6.1.0) using the human UniProt (SwissProt) database. An unspecific search was conducted using a peptide and protein FDR at 0.01 and 0.05, respectively. Peptide site-FDR was set to 0.01 min and max peptide length was set to 7 and 50, respectively. The HCD-MS/MS spectra were searched with Oxidation (M); Gln à pyro-Glu; Glu à pyro-Glu; Amidated (C-term); Acetyl (N-term) as variable modifications. Precursor ion tolerance was set to 10 ppm and MS/MS tolerance at 0.03 Da.

## In situ hybridization and immunohistochemistry

Adipose tissue samples were collected from five Genoskin donors, trimmed to ~5 mm in diameter and fixed in 10% neutral buffered formalin (VWR International) for approximately 48h. After fixation, the samples were processed and embedded in paraffin. Sections of 10 µm thickness were mounted on SuperFrost Plus slides (VWR International).

*NPY1R* mRNA was detected with RNAscope *in situ* hybridization (ISH) combined with immunohistochemical (IHC) staining of either PGP9.5 or Perilipin 1 on a Ventana Ultra Discovery autostainer (Roche). In brief, sections were baked, deparaffinized, rehydrated and underwent heat-induced epitope retrieval (HIER) in CC1 buffer with pH 8.4 at 97°C for 24 min (all reagents from Roche), followed by incubation with the *NPY1R* RNAscope probe (ACD) listed in **Supplementary Table 3**. Upon amplification according to the manufacturer's instructions, the ISH signal was developed with Discovery Rhodamine Kit (Roche). Thereafter sections were denatured in CC2 buffer with pH 6 at 95°C for 8 minutes, previous peroxidase activity was quenched with Discovery inhibitor, and unspecific antibody binding was blocked with TNB blocking buffer prior to incubation with the primary antibodies diluted in TNB buffer (rabbit anti-PGP9.5 or rabbit anti-Perilipin 1, see **Supplementary Table 3**). These primary antibodies were subsequently detected with anti-rabbit HQ (Roche) followed by HRP-labelled anti-HQ (Roche) and finally visualized with either the Discovery FAM kit (PGP9.5, Roche) or Discovery Cy5 kit (Perilipin 1, Roche). Slides were counterstained with DAPI (VWR international), and cover glasses were mounted with Fluorescent Mounting Medium (Agilent Dako). A RNAscope probe targeting RHO (ACD, see **Supplementary Table 3**) was used as negative control for the *NPY1R* ISH signal. As negative control for IHC staining of PGP9.5 and Perilipin 1, the primary antibodies were replaced with either rabbit IgG (see **Supplementary Table 3**) or TNB buffer.

Additionally, IHC staining of Perilipin 1 was combined with IHC staining of PGP9.5. This was also performed on a Ventana Ultra Discovery autostainer (Roche). In brief, the slides were baked, deparaffinized, rehydrated and HIER was performed in CC1 buffer with pH 8.4 at 95°C for 24 min. Endogenous peroxidase activity was blocked with Discovery inhibitor, and nonspecific antibody binding was blocked with TNB blocking buffer prior to incubation with the rabbit anti-Perilipin 1 antibody (**Supplementary Table 3**) diluted in TNB. This antibody was subsequently detected with BrightVision poly-HRP-anti rabbit IgG polymer (VWR international) and the Discovery Cy5 kit (Roche). Sections were then incubated in CC2 buffer with pH 6 at 95°C for 8 minutes. Peroxidase activity was quenched with Discovery inhibitor prior to

incubation with the second primary rabbit anti-PGP9.5 antibody (**Supplementary Table 3**), also diluted in TNB buffer. The second primary antibody was subsequently detected with BrightVision poly-HRP-anti rabbit IgG polymer (VWR international) followed by Discovery Rhodamine Kit (Roche). Counterstaining and mounting of cover glasses was done as described above. As negative control the primary antibodies were replaced with rabbit IgG.
Digital whole-slide images of all stained sections were captured on a VS200 slide scanner (Olympus) according to the manufacturer's instructions.

## Statistical analysis

For plotting of Correlation graphs (**Figure 4A-D**) free fatty acid and cAMP levels (**Figure 5**) we used GraphPad Prism Software (9.0.1).
Correlation values were determined by computing the pseudobulk gene expression for each donor in adipocytes and correlating these values with the clinical information. Fitted curves were plotted using a built-in GraphPad Prism XY analysis tool for "simple linear regression" showing 95% confidence interval.
Interpolated values for measuring cAMP levels were calculated using a built-in GraphPad Prism XY analysis tool for "nonlinear regression (curve fit)" with the "Standard curves to interpolate Sigmoidal, 4PL, X is concentration" calculation pre-set and the measured standards. Interpolated values for measuring of fatty acids were calculated using a built-in GraphPad Prism XY analysis tool for "Simple Linear Regression" with "Interpolated unknowns from standard curve" enabled and the measured standards.

# Conflicts of interest

The authors declared the following potential conflicts of interest with respect to research, authorship, and/or publication of this article: Julius E. R. Grothen, Jaime M. Martinez, Nikos Sidiropoulos, Jette W. Platou, Jette Mandelbaum, Pia Rothe, Henning Hvid, Mads Grønborg, Christian Toft Madsen and Thomas Å. Pedersen were all working at Novo Nordisk during their participation in the project, and as such were paid employees at Novo Nordisk. Novo Nordisk is a pharmaceutical company with a portfolio including drugs treating diabetes and obesity.

Zachary Gerhart-Hines is Chief Technology Officer for Embark Laboratories, a spinout company from Embark Biotech. Embark Laboratories develops therapeutics for the treatment of diabetes and obesity.
All other authors declare no competing interest associated with this manuscript.

# Acknowledgements

We acknowledge Mie Mechta, Kristoffer Lihme Egerod, Lars Roed Ingerslev, Oliver Knights Møller and The Single-Cell Omics platform (SCOP) at the Novo Nordisk Foundation Center for Basic Metabolic Research for technical and computational expertise, support and sequencing of the single nuclei RNA libraries.
We would like to thank Bente Kiens, Jørgen Wojtaszewski and Erik A. Richter from Department of Nutrition, Exercise and Sports, The August Krogh Section for Human and Molecular Physiology, University of Copenhagen, Copenhagen, Denmark for contributing the samples for the peptide enrichment analysis.
We would like to thank Bente Stallknecht for here contribution to the original clinical study by Bruun et al. 2006 [17]. We would like to thank Bjørn Richelsen for academic discussions related to the original study [17]. The original clinical study collecting the human samples was supported by the Novo Nordisk Foundation, Konsul J. Fogh-Nielsens Legat, and The Danish Medical Research Council (22-02-0527). The present study was funded and carried out in part by Novo Nordisk A/S. J.E.R.G. was partially funded by an Industrial PhD Student Grant (Innovation Fund Denmark, grant number 0153-00128B) and Novo Nordisk A/S. This project has received funding from the European Research Council (ERC) under the European Union's Horizon 2020 Research and Innovation Programme (grant agreement no. 639382 and 101088636 to Z.G.H.). The Novo Nordisk Foundation Center for Basic Metabolic Research is an independent research center at the University of Copenhagen, partially funded by an unrestricted donation from the Novo Nordisk Foundation (NNF18CC0034900 and NNF23SA0084103).

# References

1. Hagberg, C.E. and K.L. Spalding, *White adipocyte dysfunction and obesity-associated pathologies in humans.* Nature Reviews Molecular Cell Biology, 2024. **25**(4): p. 270-289 DOI: 10.1038/s41580-023-00680-1.

2. Kusminski, C.M., P.E. Bickel, and P.E. Scherer, *Targeting adipose tissue in the treatment of obesity-associated diabetes.* Nature Reviews Drug Discovery, 2016. **15**(9): p. 639-660 DOI: 10.1038/nrd.2016.75.
3. Neeland, I.J., P. Poirier, and J.-P. Després, *Cardiovascular and Metabolic Heterogeneity of Obesity.* Circulation, 2018. **137**(13): p. 1391-1406 DOI: doi:10.1161/CIRCULATIONAHA.117.029617.
4. Guilherme, A., et al., *Adipocyte dysfunctions linking obesity to insulin resistance and type 2 diabetes.* Nature Reviews Molecular Cell Biology, 2008. **9**(5): p. 367-377 DOI: 10.1038/nrm2391.
5. Mann, J.P. and D.B. Savage, *What lipodystrophies teach us about the metabolic syndrome.* J Clin Invest, 2019. **129**(10): p. 4009-4021 DOI: 10.1172/jci129190.
6. Rydén, M., et al., *Insulin action is severely impaired in adipocytes of apparently healthy overweight and obese subjects.* J Intern Med, 2019. **285**(5): p. 578-588 DOI: 10.1111/joim.12887.
7. Miyazaki, Y., et al., *Effect of Pioglitazone on Abdominal Fat Distribution and Insulin Sensitivity in Type 2 Diabetic Patients.* The Journal of Clinical Endocrinology & Metabolism, 2002. **87**(6): p. 2784-2791 DOI: 10.1210/jcem.87.6.8567.
8. Dumbell, R. and R.D. Cox, *The genetics of adipose tissue metabolism.* R Soc Open Sci, 2024. **11**(2): p. 231478 DOI: 10.1098/rsos.231478.
9. Huang, L.O., et al., *Genome-wide discovery of genetic loci that uncouple excess adiposity from its comorbidities.* Nature Metabolism, 2021. **3**(2): p. 228-243 DOI: 10.1038/s42255-021-00346-2.
10. Loos, R.J.F. and G.S.H. Yeo, *The genetics of obesity: from discovery to biology.* Nature Reviews Genetics, 2022. **23**(2): p. 120-133 DOI: 10.1038/s41576-021-00414-z.
11. Shungin, D., et al., *New genetic loci link adipose and insulin biology to body fat distribution.* Nature, 2015. **518**(7538): p. 187-196 DOI: 10.1038/nature14132.
12. Lotta, L.A., et al., *Integrative genomic analysis implicates limited peripheral adipose storage capacity in the pathogenesis of human insulin resistance.* Nature Genetics, 2017. **49**(1): p. 17-26 DOI: 10.1038/ng.3714.
13. Nielsen, T.S., et al., *Dissecting adipose tissue lipolysis: molecular regulation and implications for metabolic disease.* Journal of Molecular Endocrinology, 2014. **52**(3): p. R199-R222 DOI: 10.1530/jme-13-0277.
14. Rydén, M. and P. Arner, *Subcutaneous Adipocyte Lipolysis Contributes to Circulating Lipid Levels.* Arteriosclerosis, Thrombosis, and Vascular Biology, 2017. **37**(9): p. 1782-1787 DOI: doi:10.1161/ATVBAHA.117.309759.
15. Arner, P., et al., *Weight Gain and Impaired Glucose Metabolism in Women Are Predicted by Inefficient Subcutaneous Fat Cell Lipolysis.* Cell Metabolism, 2018. **28**(1): p. 45-54.e3 DOI: https://doi.org/10.1016/j.cmet.2018.05.004.
16. Stroh, A.M. and K.I. Stanford, *Exercise-induced regulation of adipose tissue.* Curr Opin Genet Dev, 2023. **81**: p. 102058 DOI: 10.1016/j.gde.2023.102058.
17. Bruun, J.M., et al., *Diet and exercise reduce low-grade inflammation and macrophage infiltration in adipose tissue but not in skeletal muscle in severely obese subjects.* American Journal of Physiology-Endocrinology and Metabolism, 2006. **290**(5): p. E961-E967 DOI: 10.1152/ajpendo.00506.2005.
18. Nicklas, B.J., E.M. Rogus, and A.P. Goldberg, *Exercise blunts declines in lipolysis and fat oxidation after dietary-induced weight loss in obese older women.* Am J Physiol, 1997. **273**(1 Pt 1): p. E149-55 DOI: 10.1152/ajpendo.1997.273.1.E149.
19. Emont, M.P., et al., *A single-cell atlas of human and mouse white adipose tissue.* Nature, 2022. **603**(7903): p. 926-933 DOI: 10.1038/s41586-022-04518-2.

20. Sun, W., et al., *snRNA-seq reveals a subpopulation of adipocytes that regulates thermogenesis.* Nature, 2020. **587**(7832): p. 98-102 DOI: 10.1038/s41586-020-2856-x.
21. Massier, L., et al., *An integrated single cell and spatial transcriptomic map of human white adipose tissue.* Nature Communications, 2023. **14**(1): p. 1438 DOI: 10.1038/s41467-023-36983-2.
22. White, P.J., et al., *Insulin action, type 2 diabetes, and branched-chain amino acids: A two-way street.* Mol Metab, 2021. **52**: p. 101261 DOI: 10.1016/j.molmet.2021.101261.
23. Tang, T., et al., *Receptor-specific recognition of NPY peptides revealed by structures of NPY receptors.* Science Advances, 2022. **8**(18): p. eabm1232 DOI: doi:10.1126/sciadv.abm1232.
24. Zhu, Y., et al., *Sympathetic neuropeptide Y protects from obesity by sustaining thermogenic fat.* Nature, 2024. **634**(8032): p. 243-250 DOI: 10.1038/s41586-024-07863-6.
25. Amisten, S., et al., *An atlas of G-protein coupled receptor expression and function in human subcutaneous adipose tissue.* Pharmacology & Therapeutics, 2015. **146**: p. 61-93 DOI: https://doi.org/10.1016/j.pharmthera.2014.09.007.
26. Serradeil-Le Gal, C., et al., *Characterization of NPY receptors controlling lipolysis and leptin secretion in human adipocytes.* FEBS Letters, 2000. **475**(2): p. 150-156 DOI: https://doi.org/10.1016/S0014-5793(00)01649-5.
27. Li, E., et al., *Control of lipolysis by a population of oxytocinergic sympathetic neurons.* Nature, 2024. **625**(7993): p. 175-180 DOI: 10.1038/s41586-023-06830-x.
28. Wieland, H.A., K. Willim, and H.N. Doods, *Receptor binding profiles of NPY analogues and fragments in different tissues and cell lines.* Peptides, 1995. **16**(8): p. 1389-1394 DOI: https://doi.org/10.1016/0196-9781(95)02028-4.
29. Park, C., et al., *Structural basis of neuropeptide Y signaling through Y1 receptor.* Nature Communications, 2022. **13**(1): p. 853 DOI: 10.1038/s41467-022-28510-6.
30. Stadlbauer, U., et al., *PYY3–36: Beyond food intake.* Frontiers in Neuroendocrinology, 2015. **38**: p. 1-11 DOI: https://doi.org/10.1016/j.yfrne.2014.12.003.
31. Zhang, W., M.A. Cline, and E.R. Gilbert, *Hypothalamus-adipose tissue crosstalk: neuropeptide Y and the regulation of energy metabolism.* Nutrition & Metabolism, 2014. **11**(1): p. 27 DOI: 10.1186/1743-7075-11-27.
32. Michel, M.C., et al., *XVI. International Union of Pharmacology Recommendations for the Nomenclature of Neuropeptide Y, Peptide YY, and Pancreatic Polypeptide Receptors.* Pharmacological Reviews, 1998. **50**(1): p. 143-150.
33. Madsen, C.T., et al., *Combining mass spectrometry and machine learning to discover bioactive peptides.* Nature Communications, 2022. **13**(1): p. 6235 DOI: 10.1038/s41467-022-34031-z.
34. LUNDBERG, J.M., et al., *Neuropeptide Y (NPY)-like immunoreactivity in peripheral noradrenergic neurons and effects of NPY on sympathetic function.* Acta Physiologica Scandinavica, 1982. **116**(4): p. 477-480 DOI: https://doi.org/10.1111/j.1748-1716.1982.tb07171.x.
35. Lundberg, J.M., et al., *Pharmacology of noradrenaline and neuropeptide tyrosine (NPY)-mediated sympathetic cotransmission.* Fundam Clin Pharmacol, 1990. **4**(4): p. 373-91 DOI: 10.1111/j.1472-8206.1990.tb00692.x.
36. Giordano, A., et al., *Tyrosine hydroxylase, neuropeptide Y, substance P, calcitonin gene-related peptide and vasoactive intestinal peptide in nerves of rat periovarian adipose tissue: an immunohistochemical and ultrastructural investigation.* J Neurocytol, 1996. **25**(2): p. 125-36 DOI: 10.1007/bf02284791.

37. Giordano, A., et al., *Regional-dependent Increase of Sympathetic Innervation in Rat White Adipose Tissue during Prolonged Fasting.* Journal of Histochemistry & Cytochemistry, 2005. **53**(6): p. 679-687 DOI: 10.1369/jhc.4A6566.2005.
38. Thompson, R.J., et al., *PGP 9.5--a new marker for vertebrate neurons and neuroendocrine cells.* Brain Res, 1983. **278**(1-2): p. 224-8 DOI: 10.1016/0006-8993(83)90241-x.
39. Zhong, J., et al., *adiposetissue.org: A knowledge portal integrating clinical and experimental data from human adipose tissue.* Cell Metabolism, 2025. **37**(3): p. 566-569 DOI: 10.1016/j.cmet.2025.01.012.
40. Kerr, A.G., et al., *Long-term changes in adipose tissue gene expression following bariatric surgery.* J Intern Med, 2020. **288**(2): p. 219-233 DOI: 10.1111/joim.13066.
41. Petrus, P., et al., *Transforming Growth Factor-β3 Regulates Adipocyte Number in Subcutaneous White Adipose Tissue.* Cell Rep, 2018. **25**(3): p. 551-560.e5 DOI: 10.1016/j.celrep.2018.09.069.
42. Keller, M., et al., *Genome-wide DNA promoter methylation and transcriptome analysis in human adipose tissue unravels novel candidate genes for obesity.* Mol Metab, 2017. **6**(1): p. 86-100 DOI: 10.1016/j.molmet.2016.11.003.
43. Arner, E., et al., *Adipose tissue microRNAs as regulators of CCL2 production in human obesity.* Diabetes, 2012. **61**(8): p. 1986-93 DOI: 10.2337/db11-1508.
44. Stancáková, A., et al., *Hyperglycemia and a common variant of GCKR are associated with the levels of eight amino acids in 9,369 Finnish men.* Diabetes, 2012. **61**(7): p. 1895-902 DOI: 10.2337/db11-1378.
45. Raulerson, C.K., et al., *Adipose Tissue Gene Expression Associations Reveal Hundreds of Candidate Genes for Cardiometabolic Traits.* Am J Hum Genet, 2019. **105**(4): p. 773-787 DOI: 10.1016/j.ajhg.2019.09.001.
46. Civelek, M., et al., *Genetic Regulation of Adipose Gene Expression and Cardio-Metabolic Traits.* Am J Hum Genet, 2017. **100**(3): p. 428-443 DOI: 10.1016/j.ajhg.2017.01.027.
47. Krieg, L., et al., *Multiomics reveal unique signatures of human epiploic adipose tissue related to systemic insulin resistance.* Gut, 2022. **71**(11): p. 2179-2193 DOI: 10.1136/gutjnl-2021-324603.
48. Arner, P., et al., *The epigenetic signature of systemic insulin resistance in obese women.* Diabetologia, 2016. **59**(11): p. 2393-2405 DOI: 10.1007/s00125-016-4074-5.
49. Imbert, A., et al., *Network Analyses Reveal Negative Link Between Changes in Adipose Tissue GDF15 and BMI During Dietary-induced Weight Loss.* J Clin Endocrinol Metab, 2022. **107**(1): p. e130-e142 DOI: 10.1210/clinem/dgab621.
50. Armenise, C., et al., *Transcriptome profiling from adipose tissue during a low-calorie diet reveals predictors of weight and glycemic outcomes in obese, nondiabetic subjects.* The American Journal of Clinical Nutrition, 2017. **106**(3): p. 736-746 DOI: https://doi.org/10.3945/ajcn.117.156216.
51. Winnier, D.A., et al., *Transcriptomic identification of ADH1B as a novel candidate gene for obesity and insulin resistance in human adipose tissue in Mexican Americans from the Veterans Administration Genetic Epidemiology Study (VAGES).* PLoS One, 2015. **10**(4): p. e0119941 DOI: 10.1371/journal.pone.0119941.
52. Nono Nankam, P.A., et al., *Distinct abdominal and gluteal adipose tissue transcriptome signatures are altered by exercise training in African women with obesity.* Sci Rep, 2020. **10**(1): p. 10240 DOI: 10.1038/s41598-020-66868-z.
53. Vink, R.G., et al., *Adipose tissue gene expression is differentially regulated with different rates of weight loss in overweight and obese humans.* Int J Obes (Lond), 2017. **41**(2): p. 309-316 DOI: 10.1038/ijo.2016.201.

54. Salcedo-Tacuma, D., et al., *Transcriptome dataset of omental and subcutaneous adipose tissues from gestational diabetes patients.* Sci Data, 2022. **9**(1): p. 344 DOI: 10.1038/s41597-022-01457-5.
55. MacLaren, R.E., et al., *Association of adipocyte genes with ASP expression: a microarray analysis of subcutaneous and omental adipose tissue in morbidly obese subjects.* BMC Med Genomics, 2010. **3**: p. 3 DOI: 10.1186/1755-8794-3-3.
56. Defour, M., et al., *Transcriptomic signature of fasting in human adipose tissue.* Physiol Genomics, 2020. **52**(10): p. 451-467 DOI: 10.1152/physiolgenomics.00083.2020.
57. Johansson, L.E., et al., *Differential gene expression in adipose tissue from obese human subjects during weight loss and weight maintenance.* Am J Clin Nutr, 2012. **96**(1): p. 196-207 DOI: 10.3945/ajcn.111.020578.
58. Matualatupauw, J.C., et al., *Dietary medium-chain saturated fatty acids induce gene expression of energy metabolism-related pathways in adipose tissue of abdominally obese subjects.* Int J Obes (Lond), 2017. **41**(9): p. 1348-1354 DOI: 10.1038/ijo.2017.120.
59. du Plessis, J., et al., *Association of Adipose Tissue Inflammation With Histologic Severity of Nonalcoholic Fatty Liver Disease.* Gastroenterology, 2015. **149**(3): p. 635-48.e14 DOI: 10.1053/j.gastro.2015.05.044.
60. Van Bussel, I.P.G., et al., *The impact of protein quantity during energy restriction on genome-wide gene expression in adipose tissue of obese humans.* Int J Obes (Lond), 2017. **41**(7): p. 1114-1120 DOI: 10.1038/ijo.2017.76.
61. Park, S., et al., *NPY antagonism reduces adiposity and attenuates age-related imbalance of adipose tissue metabolism.* Faseb j, 2014. **28**(12): p. 5337-48 DOI: 10.1096/fj.14-258384.
62. Bradley, R.L., J.P. Mansfield, and E. Maratos-Flier, *Neuropeptides, including neuropeptide Y and melanocortins, mediate lipolysis in murine adipocytes.* Obes Res, 2005. **13**(4): p. 653-61 DOI: 10.1038/oby.2005.73.
63. Kos, K., et al., *DPP-IV inhibition enhances the antilipolytic action of NPY in human adipose tissue.* Diabetes, Obesity and Metabolism, 2009. **11**(4): p. 285-292 DOI: https://doi.org/10.1111/j.1463-1326.2008.00909.x.
64. Valet, P., et al., *Neuropeptide Y and peptide YY inhibit lipolysis in human and dog fat cells through a pertussis toxin-sensitive G protein.* J Clin Invest, 1990. **85**(1): p. 291-5 DOI: 10.1172/jci114425.
65. Miranda, A.M.A., et al., *Selective remodelling of the adipose niche in obesity and weight loss.* Nature, 2025 DOI: 10.1038/s41586-025-09233-2.
66. Zhang, Y.-X., et al., *Adipose tissue aging is regulated by an altered immune system.* Frontiers in Immunology, 2023. **Volume 14 - 2023** DOI: 10.3389/fimmu.2023.1125395.
67. Feng, X., et al., *Integrative Analysis of Exosomal miR-452 and miR-4713 Downregulating NPY1R for the Prevention of Childhood Obesity.* Disease Markers, 2022. **2022**: p. 2843353 DOI: 10.1155/2022/2843353.
68. Hua, Y., et al., *Identification and analysis of key genes in adipose tissue for human obesity based on bioinformatics.* Gene, 2023. **888**: p. 147755 DOI: https://doi.org/10.1016/j.gene.2023.147755.
69. Willows, J.W., et al., *Visualization and analysis of whole depot adipose tissue neural innervation.* iScience, 2021. **24**(10): p. 103127 DOI: https://doi.org/10.1016/j.isci.2021.103127.
70. Kumari, R., et al., *Sympathetic NPY controls glucose homeostasis, cold tolerance, and cardiovascular functions in mice.* Cell Reports, 2024. **43**(2) DOI: 10.1016/j.celrep.2024.113674.
71. Genoskin. *Skin Donors & the Declaration of Helsinki*. 2025 [cited 2025 08 September]; Available from: https://genoskin.com/declaration-of-helsinki/.

72. Genoskin. *Collection of Biological Samples*. 2025 [cited 2025 08 September]; Available from: https://genoskin.com/declaration-of-helsinki/biological-sample/.
73. Bruun, J.M., S.B. Pedersen, and B. Richelsen, *Regulation of Interleukin 8 Production and Gene Expression in Human Adipose Tissue in Vitro1*. The Journal of Clinical Endocrinology & Metabolism, 2001. **86**(3): p. 1267-1273 DOI: 10.1210/jcem.86.3.7264.
74. Bruun, J.M., et al., *Interleukin-18 in plasma and adipose tissue: effects of obesity, insulin resistance, and weight loss.* European Journal of Endocrinology eur j endocrinol, 2007. **157**(4): p. 465-471 DOI: 10.1530/eje-07-0206.
75. Helge, J.W., et al., *Improved glucose tolerance after intensive life style intervention occurs without changes in muscle ceramide or triacylglycerol in morbidly obese subjects.* Acta Physiologica, 2011. **201**(3): p. 357-364 DOI: https://doi.org/10.1111/j.1748-1716.2010.02180.x.
76. Kristensen, M.M., et al., *miRNAs in human subcutaneous adipose tissue: Effects of weight loss induced by hypocaloric diet and exercise.* Obesity, 2017. **25**(3): p. 572-580 DOI: https://doi.org/10.1002/oby.21765.
77. Rodbell, M., *Metabolism of Isolated Fat Cells: I. Effects of Hormones on Glucose Metabolism and Lipolysis.* Journal of Biological Chemistry, 1964. **239**(2): p. 375-380.
78. Harms, M.J., et al., *Mature Human White Adipocytes Cultured under Membranes Maintain Identity, Function, and Can Transdifferentiate into Brown-like Adipocytes.* Cell Reports, 2019. **27**(1): p. 213-225.e5 DOI: https://doi.org/10.1016/j.celrep.2019.03.026.
79. Au - Alexandersson, I., M.J. Au - Harms, and J. Au - Boucher, *Isolation and Culture of Human Mature Adipocytes Using Membrane Mature Adipocyte Aggregate Cultures (MAAC).* JoVE, 2020(156): p. e60485 DOI: doi:10.3791/60485.
80. Rogal, J., et al., *Autologous Human Immunocompetent White Adipose Tissue-on-Chip.* Advanced Science, 2022. **9**(18): p. 2104451 DOI: https://doi.org/10.1002/advs.202104451.
81. Hong, S.J., et al., *Response of human mature adipocytes to hypoxia-reoxygenation.* Cytotherapy, 2014. **16**(12): p. 1656-1665 DOI: https://doi.org/10.1016/j.jcyt.2014.07.008.
82. Martelotto, L.G.M.L., *Frankenstein' protocol for nuclei isolation from fresh and frozen tissue for snRNAseq.* protocols.io, 2020 DOI: https://dx.doi.org/10.17504/protocols.io.bqxymxpw.
83. Zheng, G.X.Y., et al., *Massively parallel digital transcriptional profiling of single cells.* Nature Communications, 2017. **8**(1): p. 14049 DOI: 10.1038/ncomms14049.
84. Srivastava, A., et al., *Alevin efficiently estimates accurate gene abundances from dscRNA-seq data.* Genome Biology, 2019. **20**(1): p. 65 DOI: 10.1186/s13059-019-1670-y.
85. He, D., et al., *Alevin-fry unlocks rapid, accurate and memory-frugal quantification of single-cell RNA-seq data.* Nature Methods, 2022. **19**(3): p. 316-322 DOI: 10.1038/s41592-022-01408-3.
86. Genome Reference Consortium. *Genome assembly GRCh38*. NCBI RefSeq assembly GCF_000001405.26 2017; Available from: https://www.ncbi.nlm.nih.gov/datasets/genome/GCF_000001405.26/.
87. alevin-fry-tutorials. *Resolving the splicing origins of UMIs to improve the specificity of single-cell RNA-seq transcriptome mapping with alevin-fry*. 2021 [cited 2021 22-Nov]; Available from: https://combine-lab.github.io/alevin-fry-tutorials/2021/improving-txome-specificity/.
88. Griffiths, J.A., et al., *Detection and removal of barcode swapping in single-cell RNA-seq data.* Nature Communications, 2018. **9**(1): p. 2667 DOI: 10.1038/s41467-018-05083-x.

89. Lun, A.T.L., et al., *EmptyDrops: distinguishing cells from empty droplets in droplet-based single-cell RNA sequencing data.* Genome Biology, 2019. **20**(1): p. 63 DOI: 10.1186/s13059-019-1662-y.
90. Lun, A., et al. *DropletUtils - Utilities for Handling Single-Cell Droplet Data*. 2017 [cited 2021 22-Nov]; Available from: https://bioconductor.org/packages/release/bioc/html/DropletUtils.html.
91. Pagès, H., et al. *AnnotationDbi - Manipulation of SQLite-based annotations in Bioconductor*. 2007 [cited 2021 22-Nov]; Available from: https://bioconductor.org/packages/release/bioc/html/AnnotationDbi.html.
92. Germain, P., et al., *Doublet identification in single-cell sequencing data using scDblFinder [version 2; peer review: 2 approved]*. F1000Research, 2022. **10**(979) DOI: 10.12688/f1000research.73600.2.
93. Germain, P.-L. and A. Lun. *scDblFinder*. 2019 [cited 2021 22-Nov]; Available from: https://bioconductor.org/packages/release/bioc/html/scDblFinder.html.
94. Hafemeister, C. and R. Satija, *Normalization and variance stabilization of single-cell RNA-seq data using regularized negative binomial regression.* Genome Biology, 2019. **20**(1): p. 296 DOI: 10.1186/s13059-019-1874-1.
95. Facco, E., et al., *Estimating the intrinsic dimension of datasets by a minimal neighborhood information.* Scientific Reports, 2017. **7**(1): p. 12140 DOI: 10.1038/s41598-017-11873-y.
96. Traag, V.A., L. Waltman, and N.J. van Eck, *From Louvain to Leiden: guaranteeing well-connected communities.* Scientific Reports, 2019. **9**(1): p. 5233 DOI: 10.1038/s41598-019-41695-z.
97. Hao, Y., et al., *Integrated analysis of multimodal single-cell data.* Cell, 2021. **184**(13): p. 3573-3587.e29 DOI: https://doi.org/10.1016/j.cell.2021.04.048.
98. Bäckdahl, J., et al., *Spatial mapping reveals human adipocyte subpopulations with distinct sensitivities to insulin.* Cell Metab, 2021. **33**(9): p. 1869-1882.e6 DOI: 10.1016/j.cmet.2021.07.018.
99. Vijay, J., et al., *Single-cell analysis of human adipose tissue identifies depot- and disease-specific cell types.* Nature Metabolism, 2020. **2**(1): p. 97-109 DOI: 10.1038/s42255-019-0152-6.
100. Maniyadath, B., et al., *Adipose tissue at single-cell resolution.* Cell Metabolism, 2023. **35**(3): p. 386-413 DOI: https://doi.org/10.1016/j.cmet.2023.02.002.
101. Jaitin, D.A., et al., *Lipid-Associated Macrophages Control Metabolic Homeostasis in a Trem2-Dependent Manner.* Cell, 2019. **178**(3): p. 686-698.e14 DOI: https://doi.org/10.1016/j.cell.2019.05.054.
102. Hildreth, A.D., et al., *Single-cell sequencing of human white adipose tissue identifies new cell states in health and obesity.* Nature Immunology, 2021. **22**(5): p. 639-653 DOI: 10.1038/s41590-021-00922-4.
103. Strieder-Barboza, C., et al., *Single-nuclei Transcriptome of Human AT Reveals Metabolically Distinct Depot-Specific Adipose Progenitor Subpopulations.* bioRxiv, 2022: p. 2022.06.29.496888 DOI: 10.1101/2022.06.29.496888.
104. AlZaim, I., et al., *Defining the Vascular Niche of Human Adipose Tissue Across Metabolic Conditions.* bioRxiv, 2024: p. 2024.09.22.610444 DOI: 10.1101/2024.09.22.610444.
105. Loft, A., et al., *Towards a consensus atlas of human and mouse adipose tissue at single-cell resolution.* Nature Metabolism, 2025. **7**(5): p. 875-894 DOI: 10.1038/s42255-025-01296-9.
106. Wolf, F.A., P. Angerer, and F.J. Theis, *SCANPY: large-scale single-cell gene expression data analysis.* Genome Biology, 2018. **19**(1): p. 15 DOI: 10.1186/s13059-017-1382-0.

107. Sherman, B.T., et al., *DAVID: a web server for functional enrichment analysis and functional annotation of gene lists (2021 update).* Nucleic Acids Res, 2022. **50**(W1): p. W216-w221 DOI: 10.1093/nar/gkac194.
108. Huang da, W., B.T. Sherman, and R.A. Lempicki, *Systematic and integrative analysis of large gene lists using DAVID bioinformatics resources.* Nat Protoc, 2009. **4**(1): p. 44-57 DOI: 10.1038/nprot.2008.211.
109. Fridjonsdottir, E., et al., *Brain Tissue Sample Stabilization and Extraction Strategies for Neuropeptidomics.* Methods Mol Biol, 2018. **1719**: p. 41-49 DOI: 10.1007/978-1-4939-7537-2_2.
110. Secher, A., et al., *Analytic framework for peptidomics applied to large-scale neuropeptide identification.* Nature Communications, 2016. **7**(1): p. 11436 DOI: 10.1038/ncomms11436.
111. Kelstrup, C.D., et al., *Rapid and Deep Proteomes by Faster Sequencing on a Benchtop Quadrupole Ultra-High-Field Orbitrap Mass Spectrometer.* Journal of Proteome Research, 2014. **13**(12): p. 6187-6195 DOI: 10.1021/pr500985w.

# Figure Graphical Abstract: NPY-NPY1R signaling in human adipose tissue.

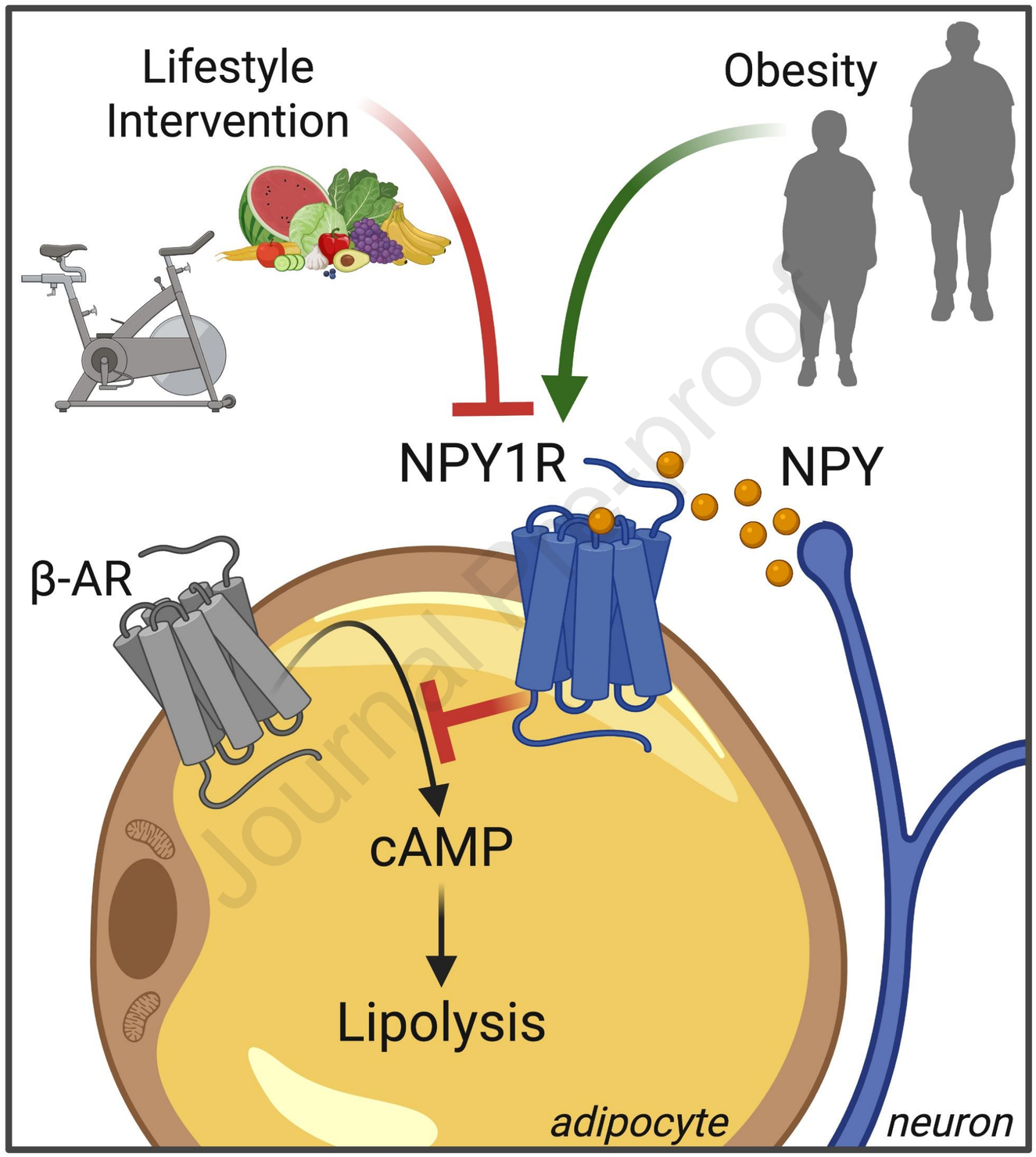


Neuropeptide Y (NPY) released by neurons in adipose tissue signals via the NPY receptor 1 (NPY1R) in human adipocytes.
NPY1R signaling results in lower cAMP levels following by β-adrenergic receptor signaling (β-AR) activation. Thus, activation of NPY1R leads to repression of stimulated lipolysis.

In adipocytes NPY1R is increased in obesity and is reduced by lifestyle intervention.

# Figure 1 – snRNAseq analysis of human subcutaneous adipose tissue before and after lifestyle intervention



A

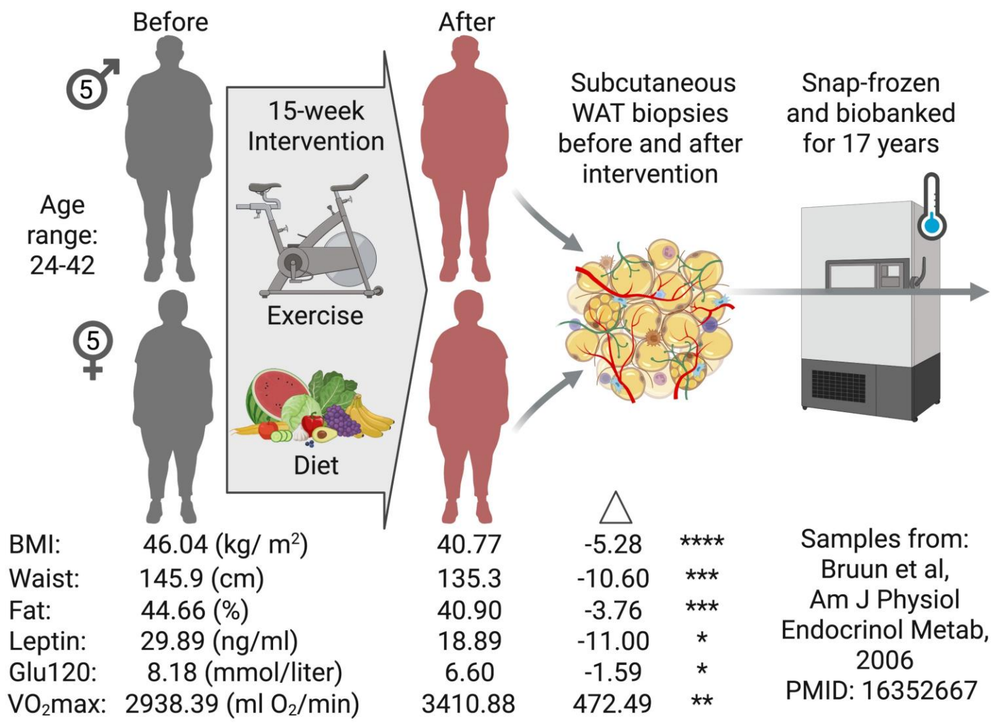


| | | | △ | |
|---|---|---|---|---|
| BMI: | 46.04 (kg/ $m^2$) | 40.77 | -5.28 | **** |
| Waist: | 145.9 (cm) | 135.3 | -10.60 | *** |
| Fat: | 44.66 (%) | 40.90 | -3.76 | *** |
| Leptin: | 29.89 (ng/ml) | 18.89 | -11.00 | * |
| Glu120: | 8.18 (mmol/liter) | 6.60 | -1.59 | * |
| $VO_2$max: | 2938.39 (ml $O_2$/min) | 3410.88 | 472.49 | ** |

B

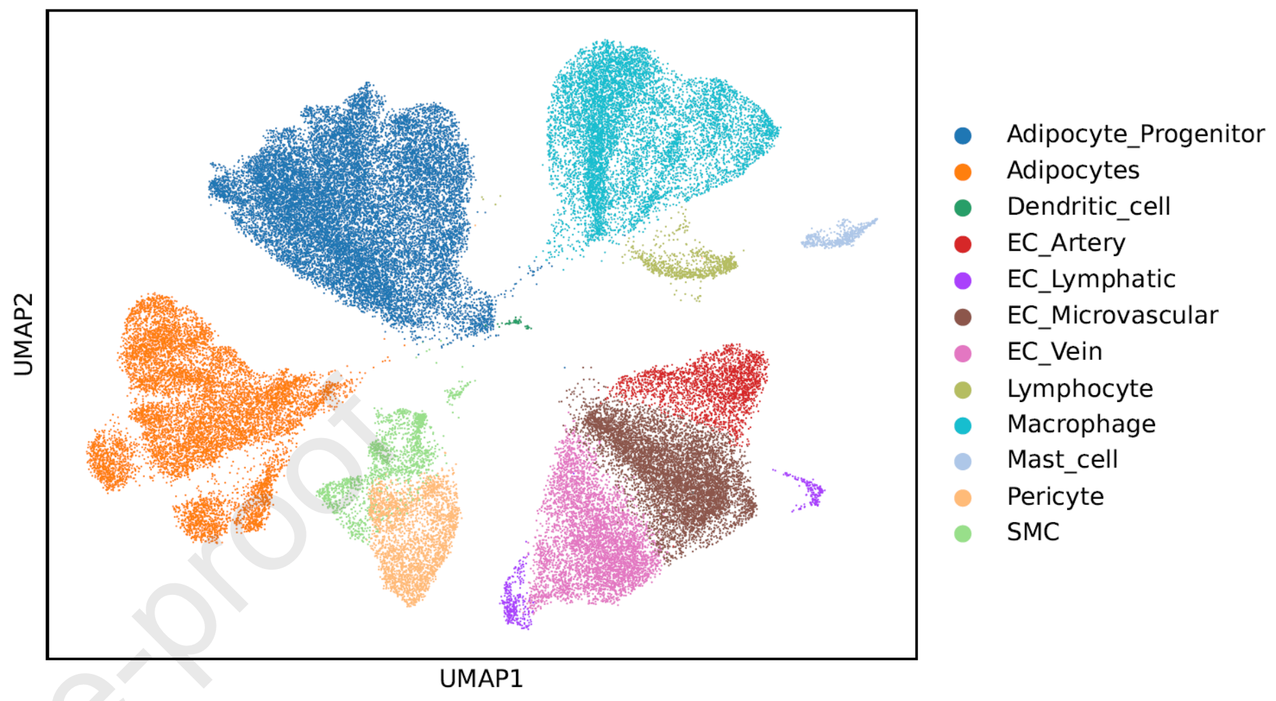


C

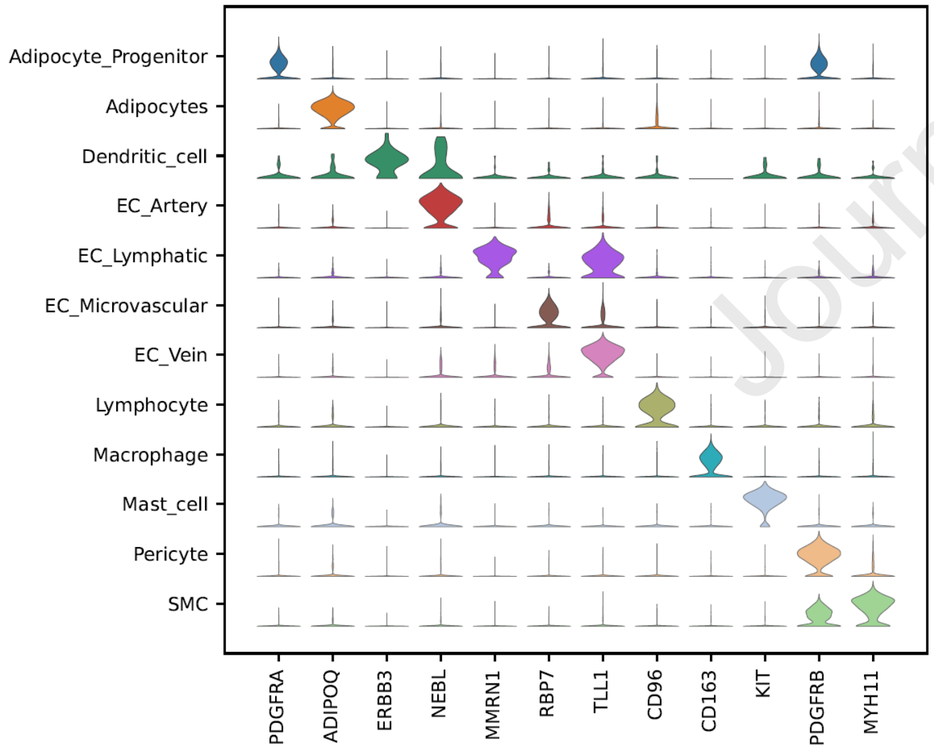


D

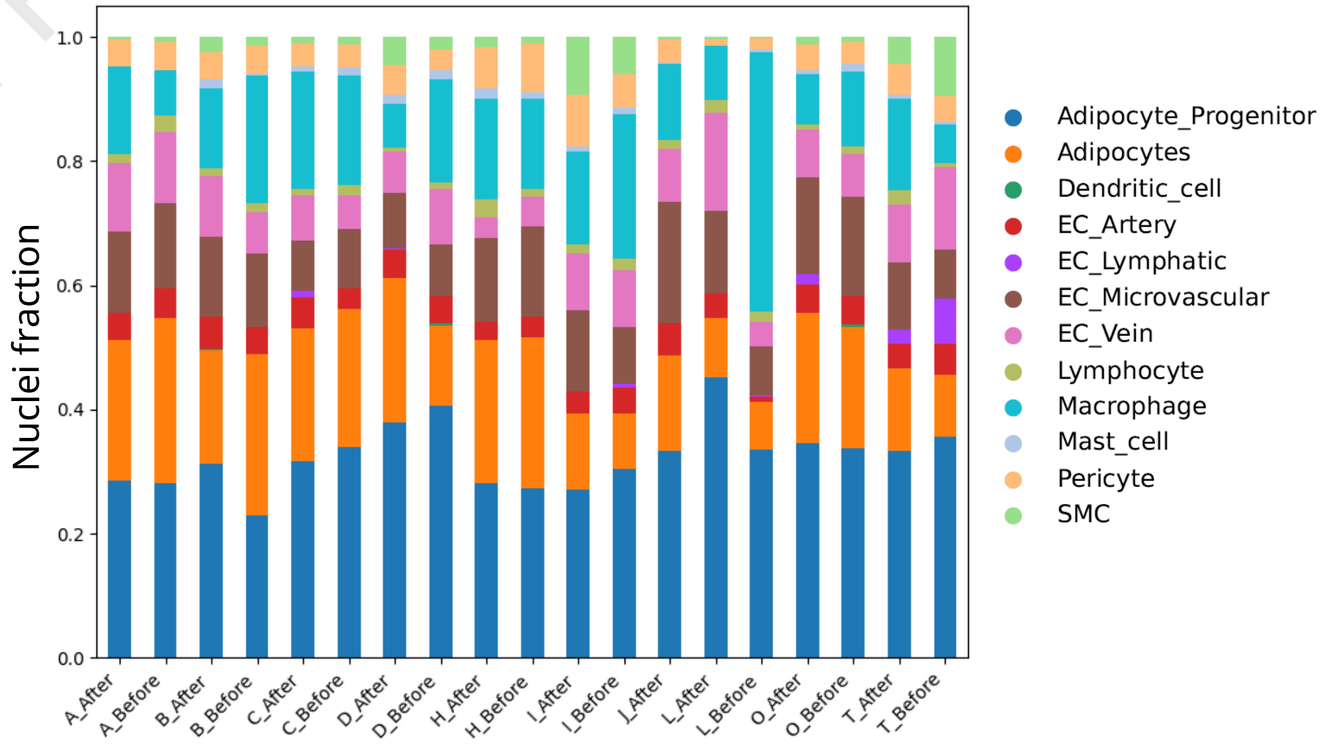


**A.** Overview of Bruun et al. 2006 study data.
**B.** UMAP containing 57,498 nuclei isolated from human subcutaneous adipose tissue from 19 samples, collected "Before" and "After" lifestyle intervention. The nuclei are separated into 12 cell-type clusters. Adipocyte Progenitors, Adipocytes, Dendritic cells, Endothelial cells Artery, Endothelial cells Lymphatic, Endothelial cells Microvascular, Endothelial cells Vein, Lymphocytes, Macrophages, Mast cells, Pericytes and Smooth Muscle cells.
**C.** Stacked Violin plot representing the expression of marker genes in the separate clusters.
**D.** Nuclei composition of the individual adipose biopsies from the 19 samples, expressed as fraction of all nuclei present in the sample.
Abbreviations: EC, Endothelial cells; SMC, Smooth muscle cells

# Figure 2 – Number of detected differentially expressed genes across cell clusters

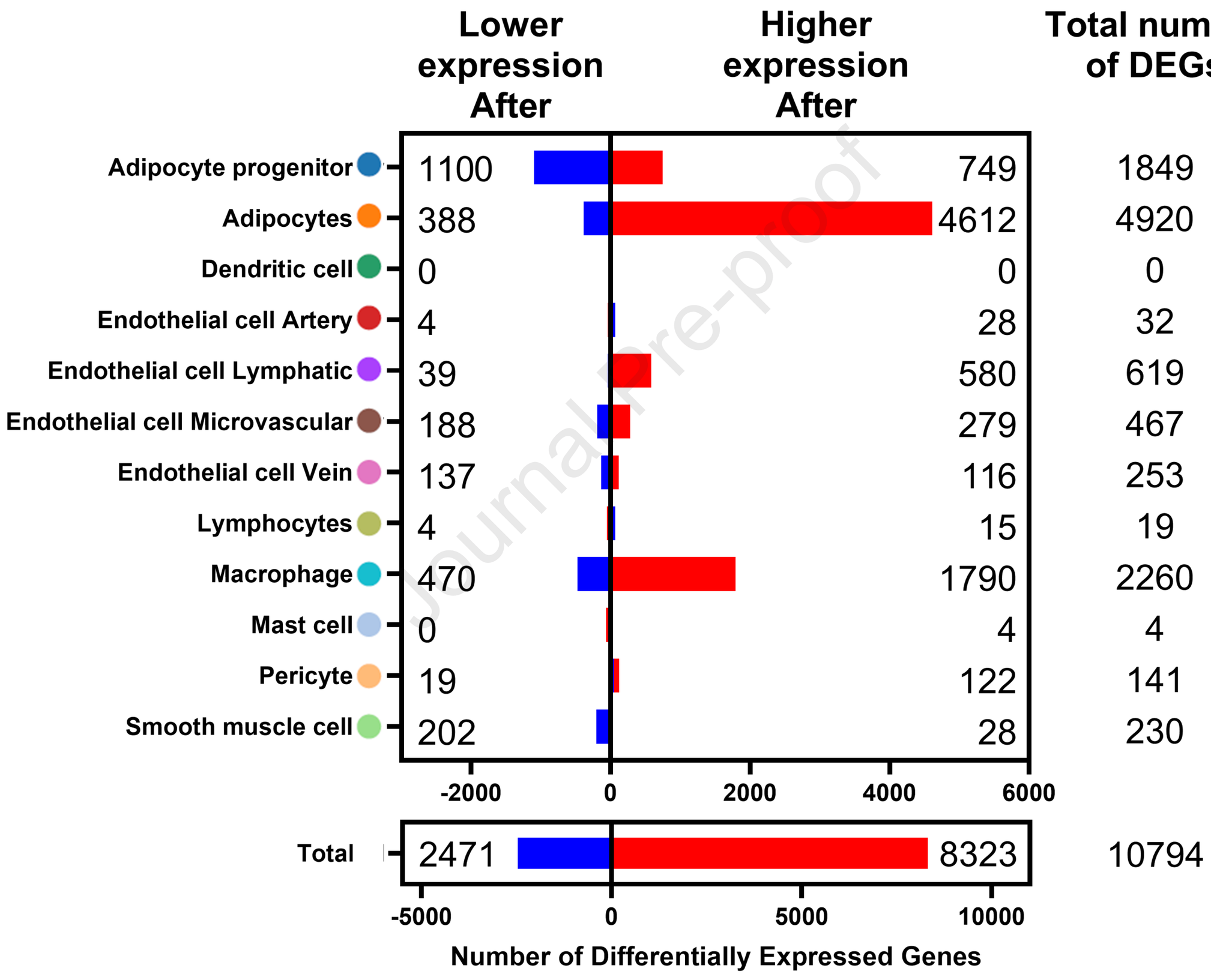

# Table 1 – Top 5 KEGG pathway analysis of differentially expressed genes in the adipocyte cluster

| Relative expression | KEGG pathway Term | Gene count, (% of total genes in pathway) | Genes identified in KEGG pathway | p-value |
|---|---|---|---|---|
| **Lower after** | hsa04923: Regulation of lipolysis in adipocytes | 7, (1.8%) | INSR; NPY1R; AQP7; ADCY6; GNAI1; MGLL; PNPLA2 | 1,80E-03 |
| **Lower after** | hsa04820: Cytoskeleton in muscle cells | 14, (3.6%) | ELN; HSPG2; SYNE1; COL3A1; FMNL2; PDLIM2; COL5A1; COL5A3; COL6A1; ITGA7; TLN2; SPTAN1; VCL; SPTBN1 | 1,81E-03 |
| **Lower after** | hsa04931: Insulin resistance | 9, (2.3%) | GYS1; MLXIPL; SLC27A1; INSR; GFPT1; OGA; PYGL; OGT; PTPRF | 2,73E-03 |
| **Lower after** | hsa04144: Endocytosis | 14, (3.6%) | RAB5B; IQSEC1; WIPF2; ASAP2; CBL; AP2A2; DNM2; EEA1; EHD2; SNX2; IL2RA; CLTCL1; PIP5K1A; SNX6 | 3,72E-03 |
| **Lower after** | hsa04520: Adherens junction | 8, (2.1%) | PDCD10; ACTN1; INSR; EP300; PTPRJ; PTPRF; VCL; NECTIN2 | 4,33E-03 |
| **Higher After** | hsa04140: Autophagy - animal | 77, (1,7%) | CALCOCO2; IRS1; MTMR14; WDR41; PTEN; IRS2; PIK3CB; WDR45; RPTOR; TBK1; CTSL; AKT2; RB1CC1; LAMP2; EPG5; PRKACA; PRKACB; MAP3K7; VPS39; SH3GLB1; ATG3; GABARAPL2; GABARAPL1; MAP2K1; DAPK2; PRKCD; ATG10; WIPI2; ATG14; ATG13; ATG12; RAB33B; MRAS; GORASP2; RRAGB; DDIT4; TAX1BP1; PIK3C3; PRKCQ; WDFY3; BIRC6; RAF1; RAB7A; PRKAA1; STX17; PIK3R4; ITPR1; PIK3R1; AMBRA1; MTMR4; HIF1A; TANK; C9ORF72; PPP2CA; PPP2CB; MAPK9; MAPK8; MAPK1; NRBF2; RPS27A; ATG7; ATG5; IGBP1; UVRAG; BNIP3; CFLAR; EIF2S1; MTOR; MAPK10; ATG16L2; ATG16L1; RHEB; RPS6KB2; VPS41; KRAS; ATG2B; BCL2L1 | 3,15E-11 |
| **Higher After** | hsa00280: Valine: leucine and isoleucine degradation | 31, (0,7%) | ACAA2; HIBADH; ABAT; AACS; ACAT1; HMGCL; MCEE; AUH; OXCT1; DBT; AOX1; MMUT; HADH; ACAA1; BCKDHA; MCCC2; HMGCS1; BCKDHB; MCCC1; ACSF3; ACADSB; HADHB; ALDH3A2; HADHA; PCCA; IVD; EHHADH; PCCB; DLD; ALDH7A1; ALDH9A1 | 2,22E-09 |
| **Higher After** | hsa03013: Nucleocytoplasmic transport | 51, (1,1%) | AHCTF1; IPO11; NUP107; PNN; IPO9; SUMO1; XPO4; XPO6; MAGOH; KPNA6; KPNA4; KPNA5; TNPO1; KPNA3; TNPO3; KPNA1; UPF2; NUP214; UPF1; SEC13; NUP133; NCBP1; NCBP2; THOC1; THOC2; SENP2; THOC7; SRRM1; EEF1A1; DDX39B; TMEM33; NUP54; NUP98; NUP58; POM121; NMD3; POM121C; NUP85; NUP42; SAP18; NUP88; RANBP2; UBE2I; NUP155; PYM1; XPO7; NUP153; MAGOHB; XPOT; RNPS1; NUP37 | 2,36E-08 |
| **Higher After** | hsa04120: Ubiquitin mediated proteolysis | 62, (1,4%) | DET1; UBE2D4; UBE2D3; UBE3A; CBLB; UBE3B; HERC4; HERC3; HERC2; CDC23; HERC1; UBE2Q2; CDC27; FBXO4; ELOC; SKP2; SKP1; FBXW8; FBXW11; FBXW7; UBE2E3; UBE2E1; UBE4A; UBE2QL1; UBE4B; PIAS2; PIAS1; DDB1; CDC34; BIRC6; ANAPC1; PRKN; CUL5; UBA6; CUL3; CUL2; CUL1; NEDD4L; XIAP; ANAPC10; RHOBTB1; COP1; VHL; RPS27A; UBE2F; UBE2I; PPIL2; SMURF1; FANCL; SIAH1; HUWE1; WWP1; UBE2G1; CUL4A; UBE2W; UBE2N; UBA3; MDM2; ERCC8; UBA1; TRIP12; CUL4B | 2,38E-08 |
| **Higher After** | hsa00640: Propanoate metabolism | 23, (0,5%) | BCKDHA; ACSS3; BCKDHB; ABAT; ACACB; ACACA; LDHB; HADHA; LDHA; MCEE; SUCLA2; PCCA; ACOX1; EHHADH; PCCB; DBT; ECHDC1; SUCLG2; SUCLG1; MMUT; ACOX3; MLYCD; DLD | 2,45E-08 |

# Figure 3 – NPY and NPY1R identified in human adipose tissue



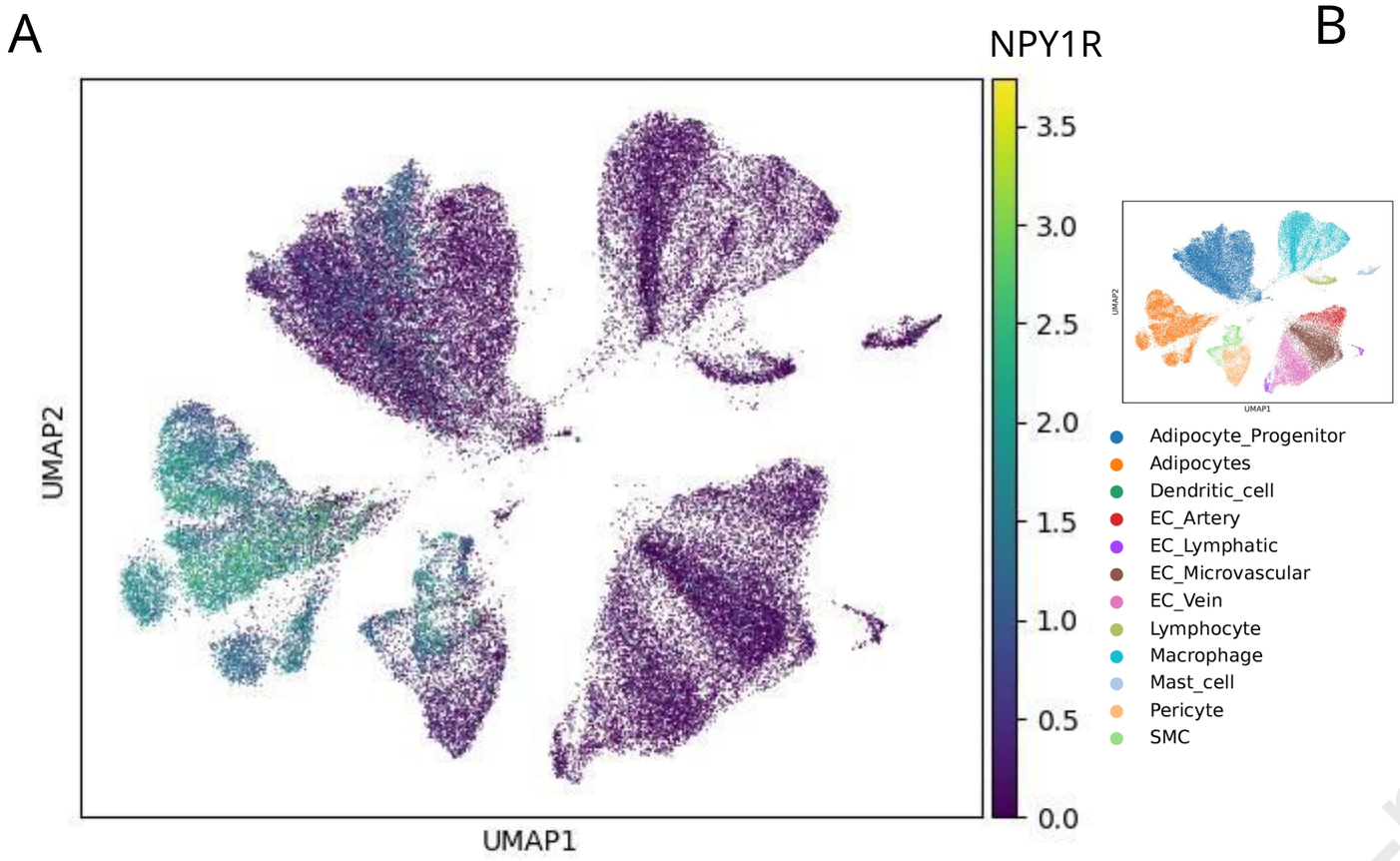


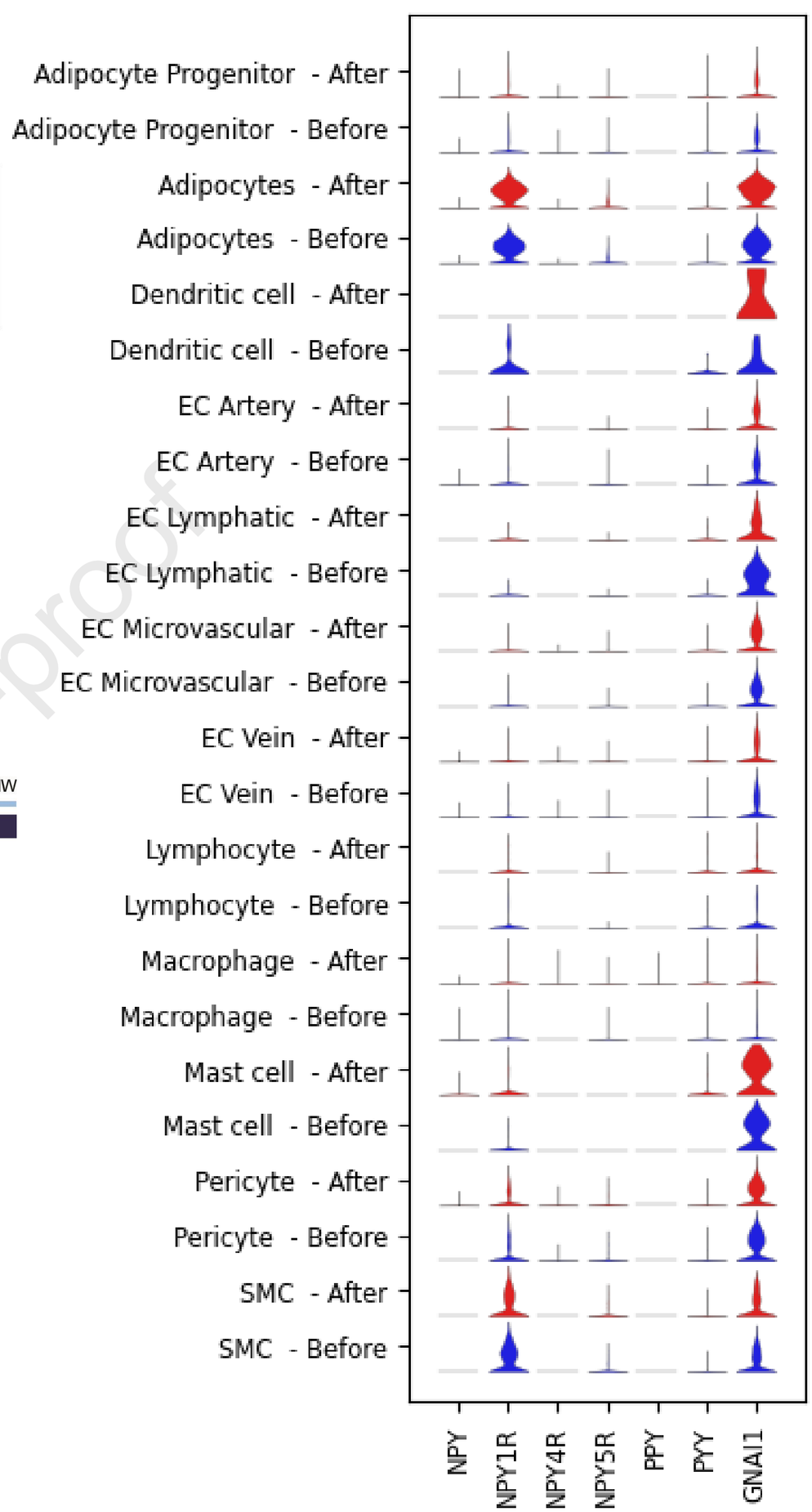


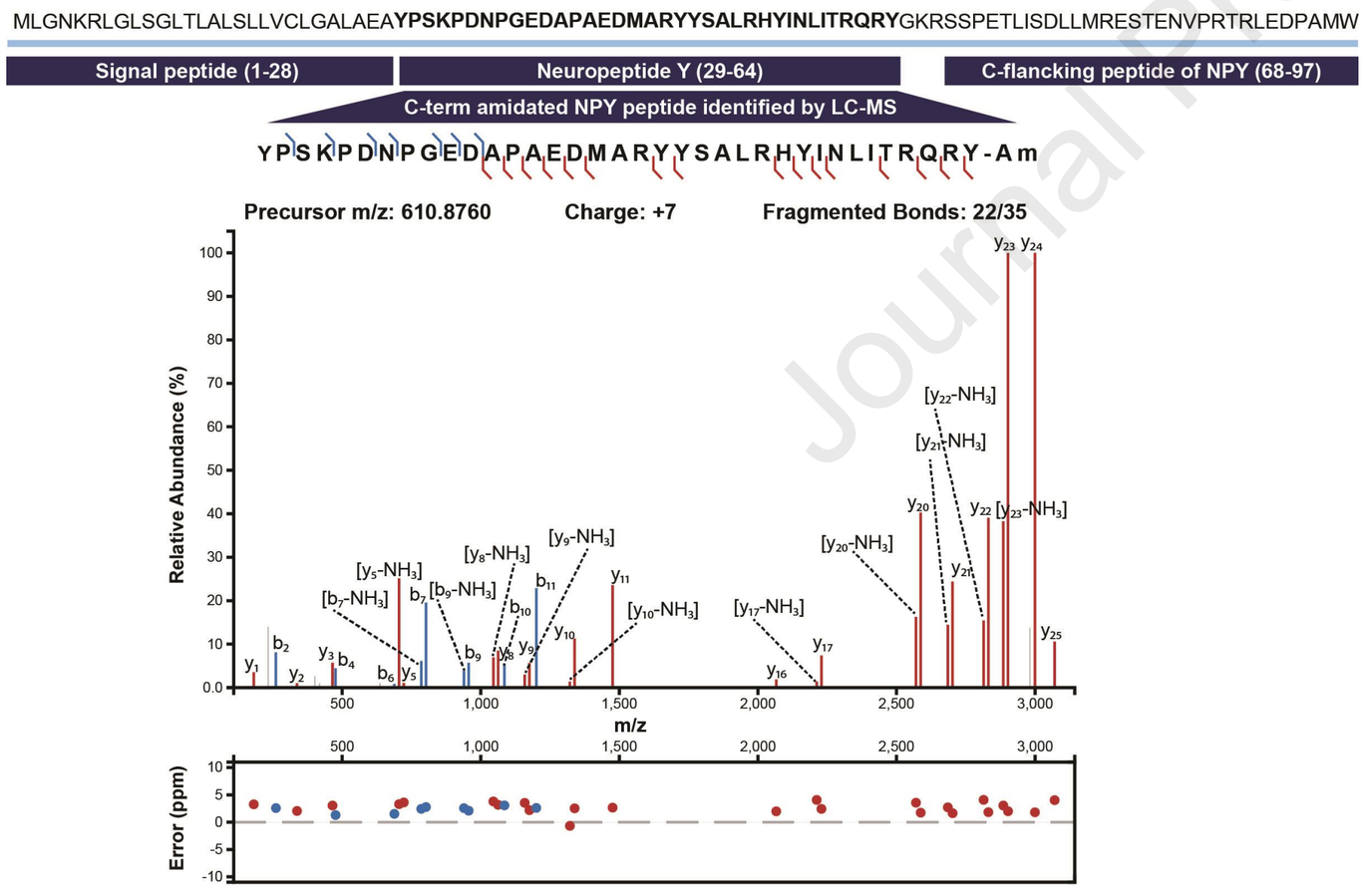


**A.** Expression of NPY1R visualized in UMAP of snRNAseq from human subcutaneous adipose tissue from
**B.** Stacked Violin plot representing the expression levels from snRNAseq analysis, of *NPY*, *NPY1R*, *NPY4R, NPY5R, PPY, PYY* and *GNAI1* across the different cell types, *NPY2R* was not detected in the snRNAseq. None of the genes were differentially expressed following lifestyle intervention.
**C.** Sequence of Pro-neuropeptide Y protein (Uniprot ID: P01303), consisting of signal peptide (1-28), neuropeptide Y (29-64) and C-flacking peptide of NPY (68-97). Highlighted in bold, C-terminal amidated NPY peptide (29-64) identified by LC-MS analysis. MS/MS spectrum showing b- and y-fragment ions used for identifying amidated NPY (top panel). Error tolerance for all fragment ions were < 5 ppm for the LC-MS analysis (bottom panel).

# Figure 4 – NPY1R and PGP9.5 in human adipose tissue

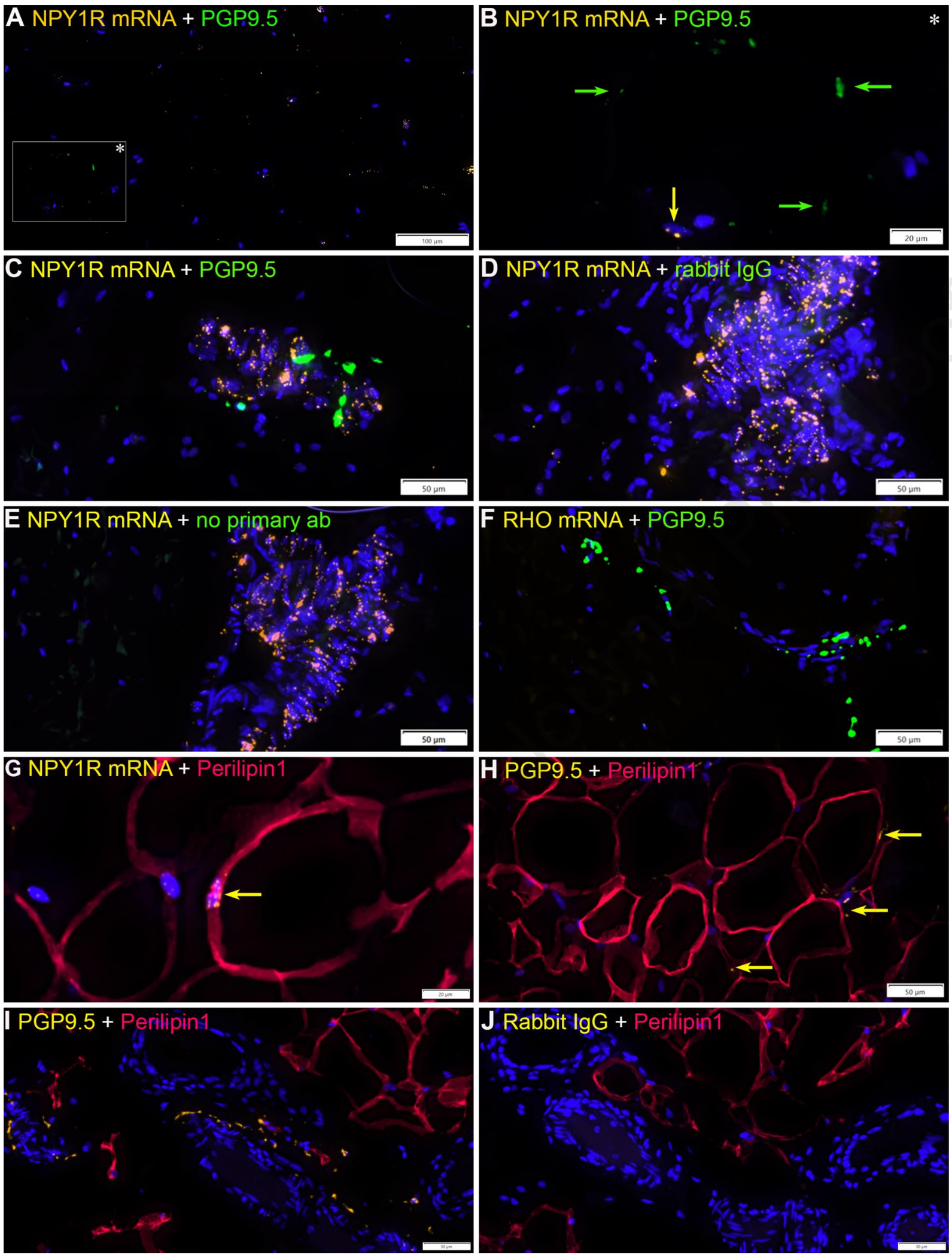


**A.** Double staining using NPY1R mRNA ISH (orange) probe and anti-PGP9.5 (green) of human adipose tissue, at 100 µm scale. Square and (*) denotes section visualized in **B.**

**B.** Subsection of **A.** staining using NPY1R mRNA ISH probe and anti-PGP9.5 of human adipose tissue, at 20 µm scale. Arrows added to denote signal (Orange – NPY1R mRNA, Green – PGP9.5).

**C.** Double staining using NPY1R mRNA ISH (orange) probe and anti-PGP9.5 (green) of blood vessels in human adipose tissue, at 50 µm scale. **D.** Comparable double stain to **C.** substituting anti-PGP9.5 with Isotype control IgG (green). **E.** comparable to **A.** without a primary antibody (green). **F.** comparable to **C.** substituting NPY1R mRNA ISH (orange) probe with RHO mRNA ISH (orange) probe.

**G.** Double staining using NPY1R mRNA ISH (orange) probe and anti-PLIN1 (red) of human adipose tissue, at 20 µm scale. Arrow added to denote signal NPY1R mRNA (orange) probe signal.

**H.** Double staining using anti-PGP9.5 (orange) and anti-PLIN1 (red) of human adipose tissue, at 50 µm scale. Arrow added to denote anti-PGP9.5 (orange).

**I.** Double staining using anti-PGP9.5 (orange) and anti-PLIN1 (red) of human adipose tissue blood vessels, at 100 µm scale. **J.** Comparable stain to **I.** substituting anti-PGP9.5 with Isotype control IgG (orange).

**A. B. C. D. E. F. G. H. I. J.** Staining was done on tissue from 5 Genoskin donors. Images are representative of the findings across samples. Blue color in all slides represent nuclei stains using DAPI.

# Figure 5 – Clinical correlation of NPY1R in human adipose tissue





A

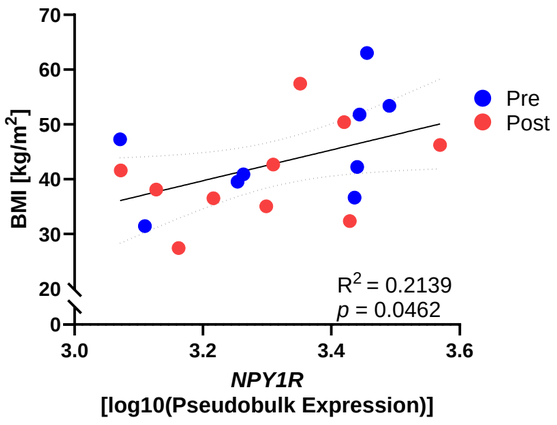


B

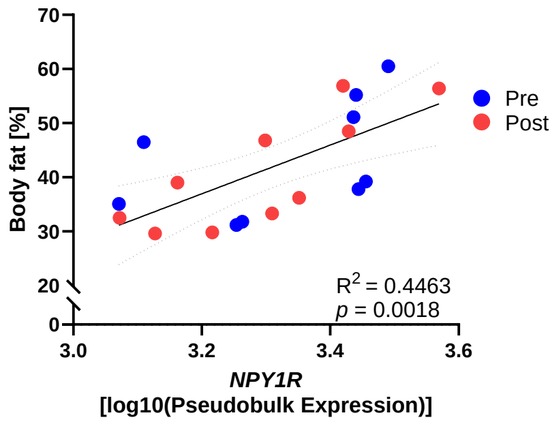


C

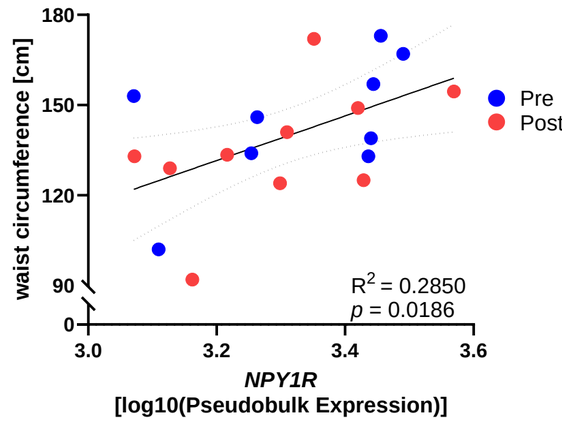


D

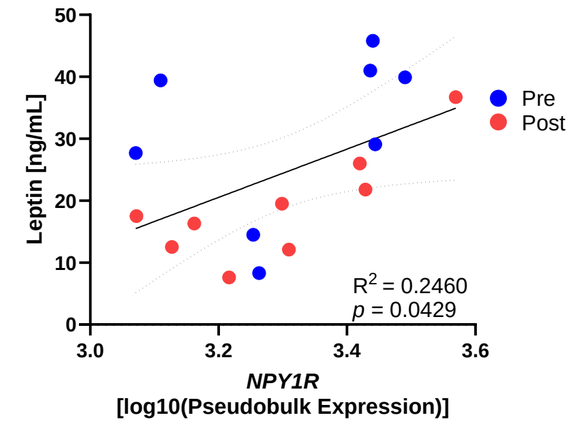


E

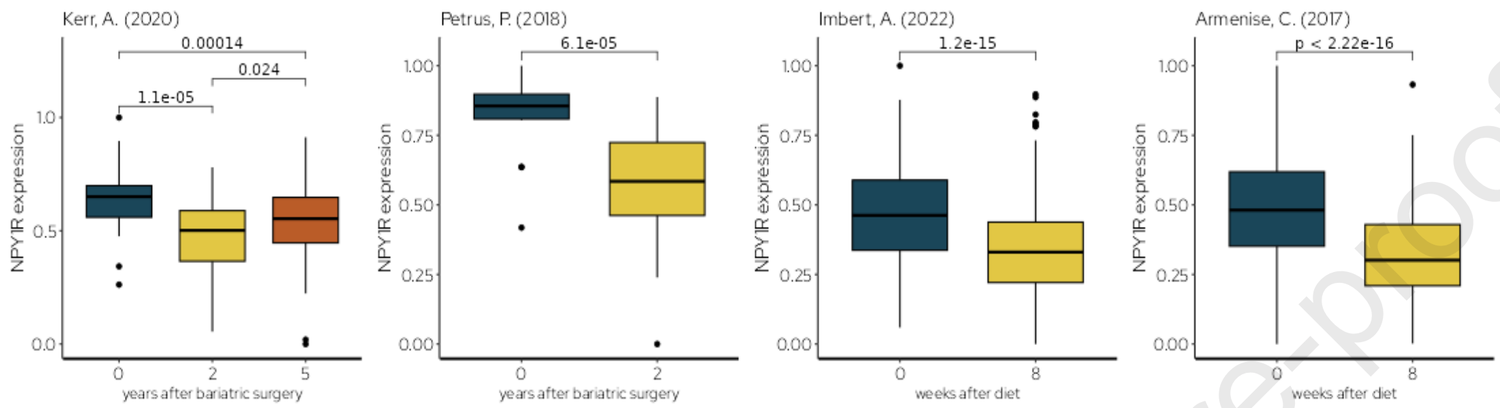


F

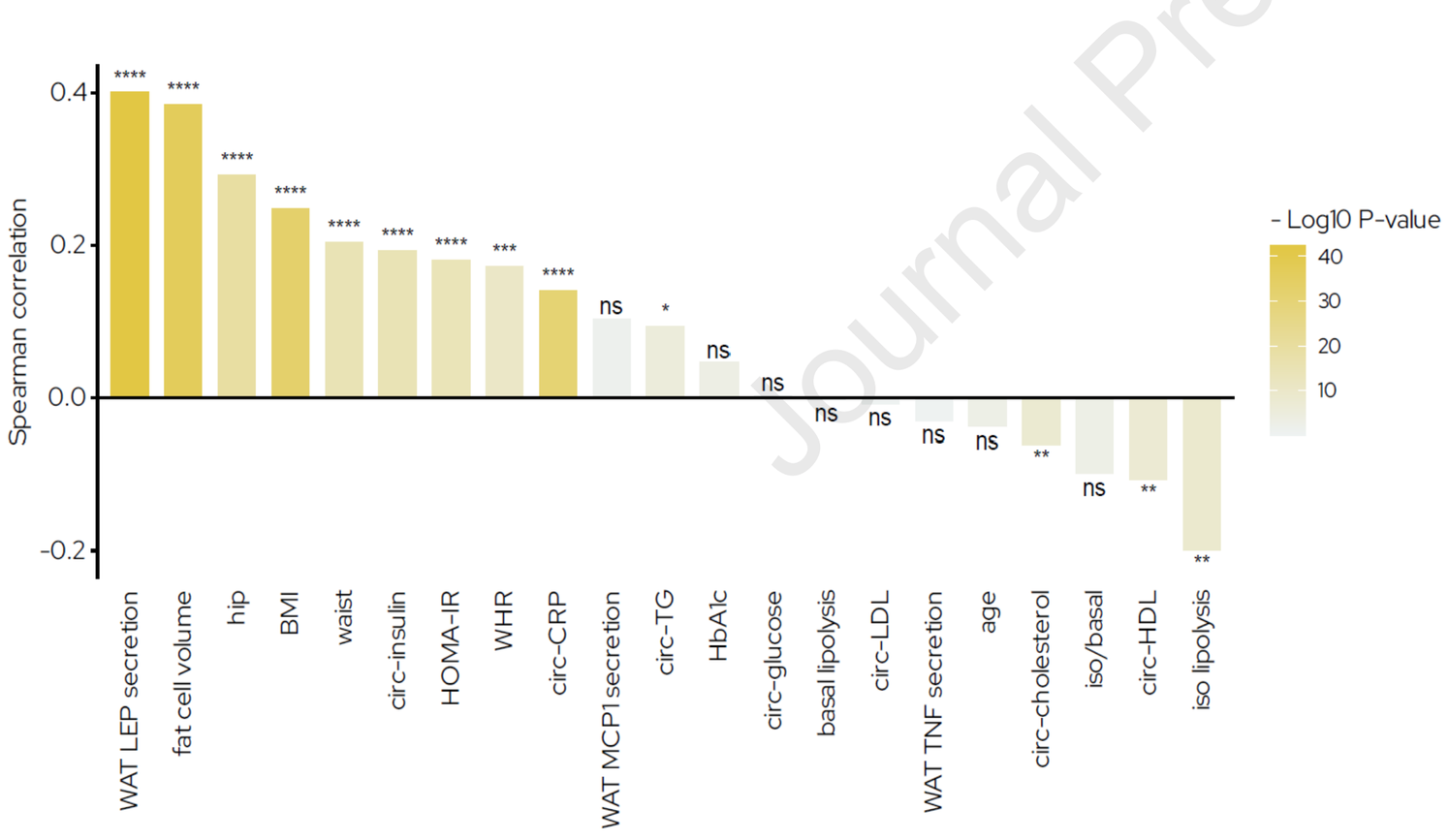


G

## BMI

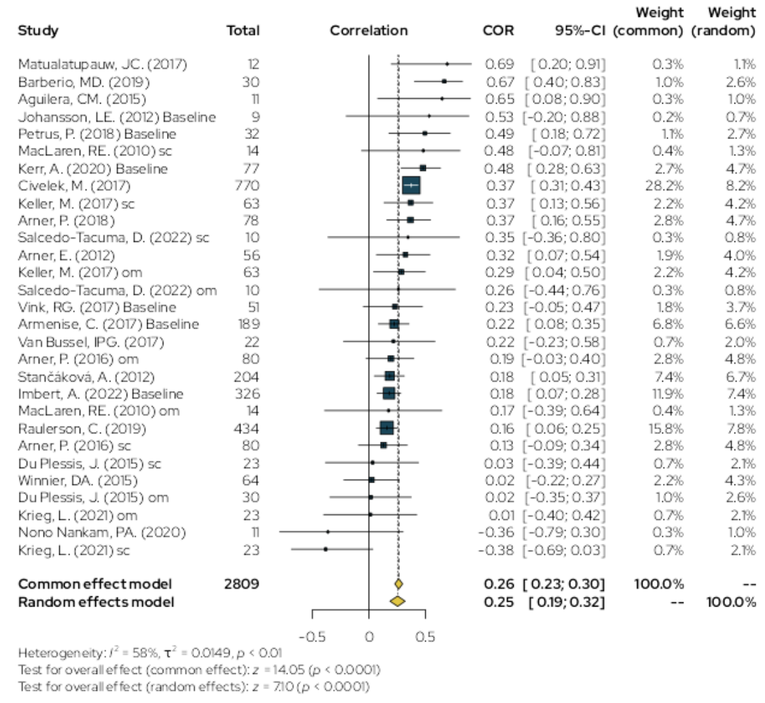


H

## Waist circumference

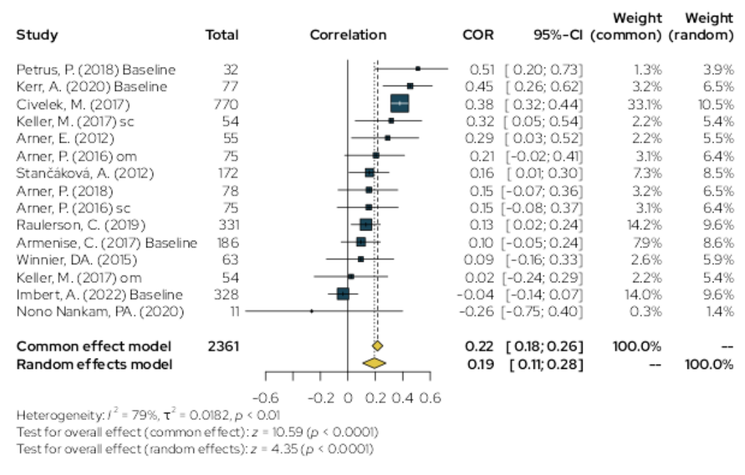


I

## WAT Leptin Secretion

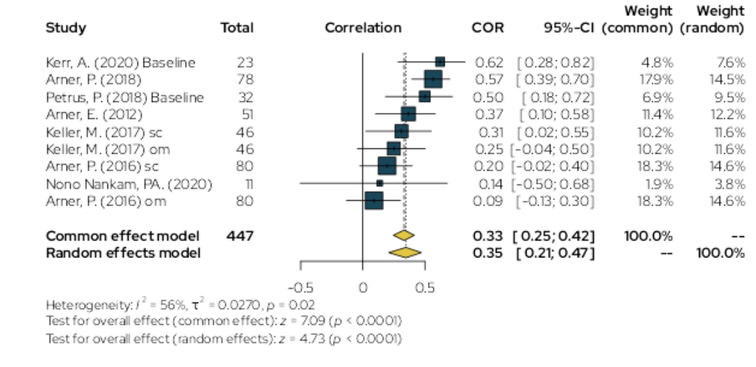


J

## Fat cell volume

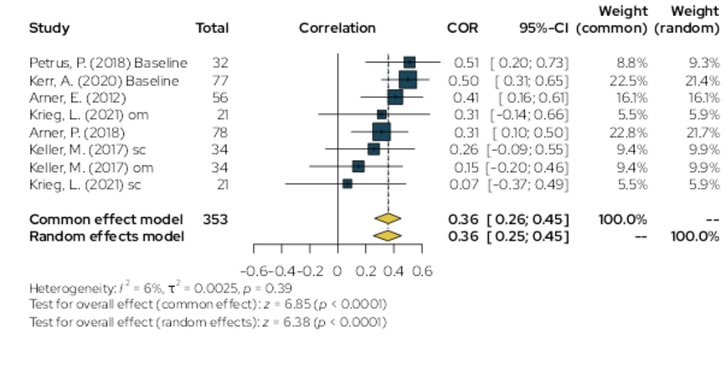


K

## Isoproterenol-induced lipolysis

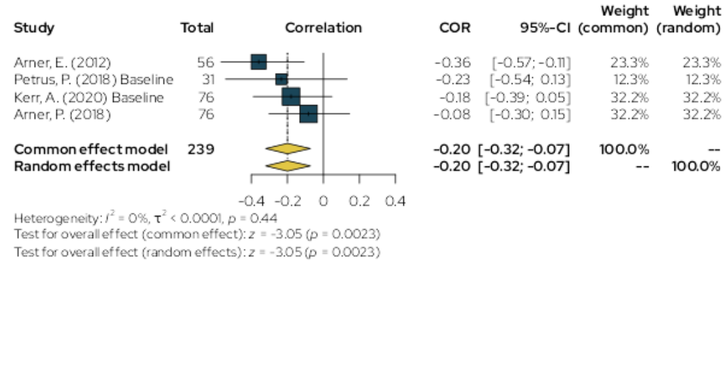

# Figure 5 – Clinical correlation of NPY1R in human adipose tissue

**A. B. C. D.** Identified significant correlations of NPY1R gene expression in adipocytes with clinical parameters. **A.** Correlation with BMI, **B.** Correlation with Body fat, **C.** Correlation with Waist circumference, and **D.** Correlation with Leptin.

**E. F. G. H. I. J. K.** Plots from adiposetissue.org knowledge portal. **E.** NPY1R expression in adipose tissue was found to decrease in weight-loss intervention studies. **F.** Correlation of NPY1R expression with clinical parameters from described on the portal. **G. H. I. J. K.** Forrest plots are shown for correlations with **G.** BMI, **H.** Waist circumference and **I.** WAT Leptin Secretion, **J.** Fat cell volume, **K.** Isoproterenol-induced lipolysis.

# Figure 6 – Neuropeptide Y response in human adipocytes

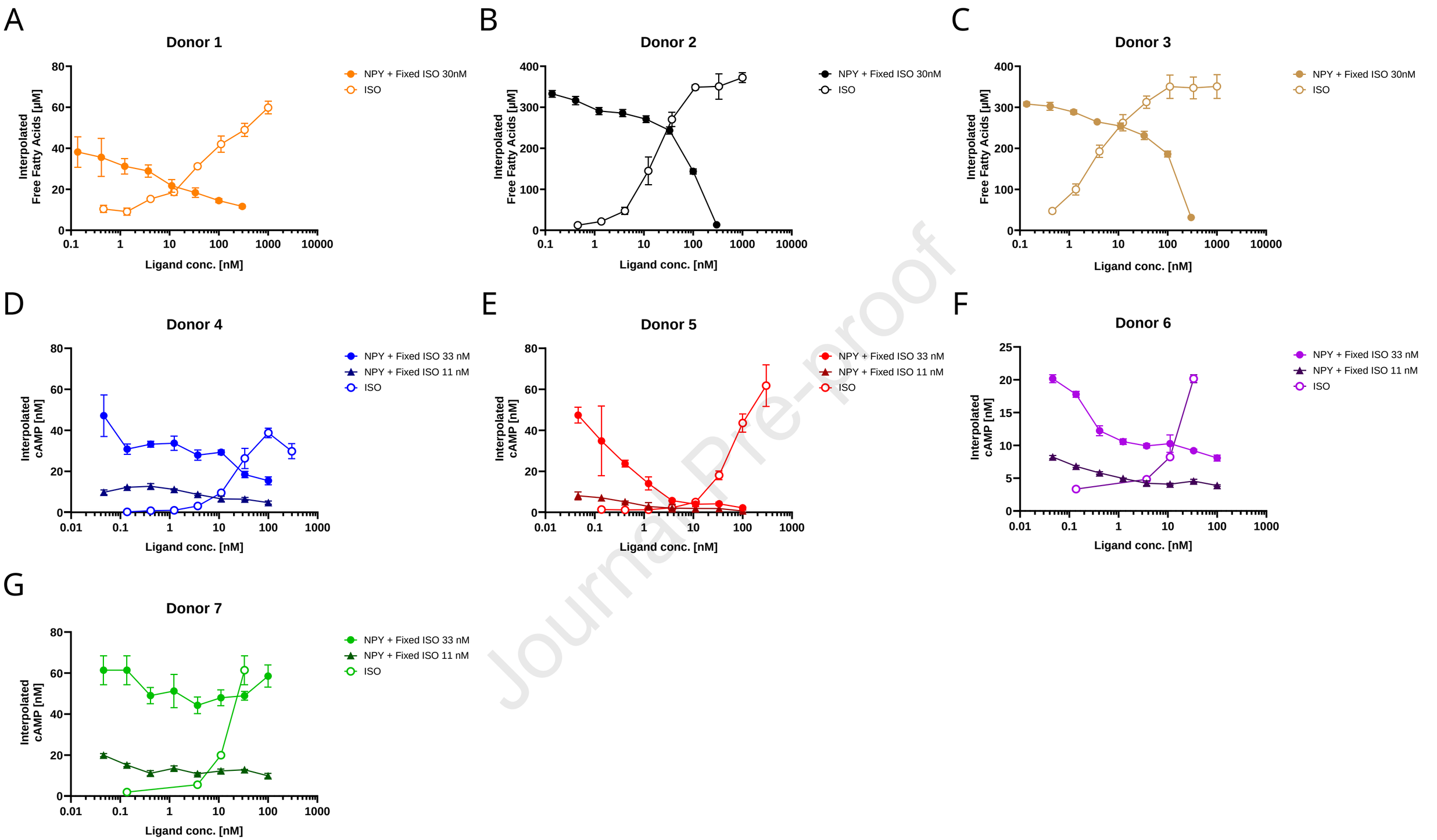


**A. B. C.** Measurement of free fatty acids released from isolated mature human adipocytes in the presence of the indicated concentration of isoproterenol (ISO) or neuropeptide Y (NPY). Assessment of NPY effect was performed at a constant ISO concentration of 30 nM.
**D. F. E. G.** cAMP levels measured in 3D cultured mature human adipocytes in the presence of the indicated concentration of isoproterenol (ISO) or neuropeptide Y (NPY). Assessment of NPY effect was performed at a constant ISO concentration of either 33 nM or 11 nM.
All graphs contain adipocytes from separate donors. First point for each ISO curve represents no ligand stimulation. Error bars represent SEM of technical replicates

**Highlights**

• Single nuclei RNAseq was performed on of human adipose tissue before and after 15-week hypocaloric diet combined with moderate physical exercise.

• Weight loss reduces Neuropeptide Y receptor Y1 (NPY1R) to enhance metabolic health

• NPY-NPY1R signaling inhibits lipolysis in human adipocytes

**Declaration of Interest Statement**

☐ The authors declare that they have no known competing financial interests or personal relationships that could have appeared to influence the work reported in this paper.

☒ The author is an Editorial Board Member/Editor-in-Chief/Associate Editor/Guest Editor for this journal and was not involved in the editorial review or the decision to publish this article.

☒ The authors declare the following financial interests/personal relationships which may be considered as potential competing interests:

The authors declared the following potential conflicts of interest with respect to research, authorship, and/or publication of this article: Julius E. R. Grothen, Jaime M. Martinez, Ni-kos Sidiropoulos, Jette W. Platou, Jette Mandelbaum, Pia Rothe, Henning Hvid, Mads Grønborg, Christian Toft Madsen and Thomas Å. Pedersen were all working at Novo Nordisk during their participation in the project, and as such were paid employees at Novo Nordisk. Novo Nordisk is a pharmaceutical company with a portfolio including drugs treating diabetes and obesity.
Zachary Gerhart-Hines is Chief Technology Officer for Embark Laboratories, a spinout company from Embark Biotech. Embark Laboratories develops therapeutics for the treatment of diabetes and obesity.
All other authors declare no competing interest associated with this manuscript.